Nano Energy 88 (2021) 106241

Contents lists available at ScienceDirect

Nano Energy

journal homepage: www.elsevier.com/locate/nanoen

Tailoring the selectivity of ultralow-power heterojunction gas sensors by noble metal nanoparticle functionalization

Oleg Lupan [a,b,c,d,*], Nicolai Ababii [b], David Santos-Carballal [e,**], Maik-Ivo Terasa [a], Nicolae Magariu [b], Dario Zappa [f], Elisabetta Comini [f], Thierry Pauporté [c], Leonard Siebert [a], Franz Faupel [g,**], Alexander Vahl [g,**], Sandra Hansen [a,**], Nora H. de Leeuw [e,h], Rainer Adelung [a,**]

[a] Functional Nanomaterials, Faculty of Engineering, Institute for Materials Science, Kiel University, Kaiserstr. 2, D-24143 Kiel, Germany
[b] Center for Nanotechnology and Nanosensors, Department of Microelectronics and Biomedical Engineering, Technical University of Moldova, 168 Stefan cel Mare Av., MD-2004 Chisinau, Republic of Moldova
[c] PSL Université, Institut de Recherche de Chimie Paris-IRCP, Chimie ParisTech, rue Pierre et Marie Curie 11, 75231 Paris Cedex 05, France
[d] Department of Physics, University of Central Florida, Orlando, FL 32816-2385, USA
[e] School of Chemistry, University of Leeds, Leeds LS2 9JT, United Kingdom
[f] Sensor Laboratory, Department of Information Engineering (DII), University of Brescia, Via Branze 38, Brescia 25123, Italy
[g] Chair for Multicomponent Materials, Faculty of Engineering, Kiel University, Kaiserstr. 2, D-24143 Kiel, Germany
[h] Department of Earth Sciences, Utrecht University, Princetonplein 8 A, 3584 CD Utrecht, The Netherlands

ARTICLE INFO

Keywords:
Nanolayered materials
Heterojunctions
Semiconductor oxides
Gas sensing
Low-energy
Ultralow power

ABSTRACT

Heterojunctions are used in solar cells and optoelectronics applications owing to their excellent electrical and structural properties. Recently, these energy-efficient systems have also been employed as sensors to distinguish between individual gases within mixtures. Through a simple and versatile functionalization approach using noble metal nanoparticles, the sensing properties of heterojunctions can be controlled at the nanoscopic scale. This work reports the nanoparticle surface functionalization of TiO_2/CuO/Cu_2O mixed oxide heterostructures, where the gas sensing selectivity of the material is tuned to achieve versatile sensors with ultra-low power consumption. Functionalization with Ag or AgPt-nanoclusters (5–15 nm diameter), changed the selectivity from ethanol to butanol vapour, whereas Pd-nanocluster functionalization shifts the selectivity from the alcohols to hydrogen. The fabricated sensors show excellent low power consumption below 1 nW. To gain insight into the selectivity mechanism, density functional theory (DFT) calculations have been carried out to simulate the adsorption of H_2, C_2H_5OH and *n*-C_4H_9OH at the noble metal nanoparticle decorated ternary heterostructure interface. These calculations also show a decrease in the work function by ~2.6 eV with respect to the pristine ternary heterojunctions. This work lays the foundation for the production of a highly versatile array of sensors of ultra-low power consumption with applications for the detection of individual gases in a mixture.

1. Introduction

Tuning the properties of semiconductor-powered devices by means of functional oxide nanomaterials is a state-of-the-art technological approach. Heterojunctions have gained attention for applications in optoelectronics and solar cells, but they can also be employed as versatile and ultra-low power gas sensors owning to the high degree of phase control at the nanoscopic level [1–6]. Previous studies on the decoration of semiconducting metal oxide nanostructures with nanoparticles (NPs), have demonstrated the versatile nature of such combined systems, e.g. in gas, UV and temperature sensors or for the discrimination of volatiles [7–9]. For example, a significant increase in sensitivity by a factor of ~60 and selectivity towards 200 ppm of ethanol vapours was achieved following surface functionalization of columnar

* Corresponding author at: Functional Nanomaterials, Faculty of Engineering, Institute for Materials Science, Kiel University, Kaiserstr. 2, D-24143 Kiel, Germany.
** Corresponding authors.
E-mail addresses: ollu@tf.uni-kiel.de, oleg.lupan@mib.utm.md (O. Lupan), d.santos-carballal@leeds.ac.uk (D. Santos-Carballal), alva@tf.uni-kiel.de (A. Vahl), sn@tf.uni-kiel.de (S. Hansen), ra@tf.uni-kiel.de (R. Adelung).

https://doi.org/10.1016/j.nanoen.2021.106241
Received 12 March 2021; Received in revised form 4 June 2021; Accepted 5 June 2021
Available online 9 June 2021

ZnO:Fe films using AgO/Ag nanoparticles [4]. This behaviour was confirmed by quantum mechanical calculations showing that $(AgO)_5$ clusters change the surface chemistry of the Fe-doped zinc oxide ZnO (10−10) surface towards ethanol detection [4]. Wang et al. [10] found that tetragonal rutile SnO_2 nanosheets decorated with an optimum amount of 3 mol% of NiO nanoparticles increases by five times the response to 100 ppm of C_2H_5OH at 260 °C, compared to the sensor containing only pure SnO_2 nanosheets. These findings were assigned to the formation of a *p*–*n* junction between the NiO nanoparticles and SnO_2 nanosheets [10]. Moreover, surface functionalisation using nanoparticles of noble metals and their alloys has been used previously to fabricate sensors for the detection of VOC molecules [9,11]. Nanometre-sized titanium dioxide (TiO_2) quantum dots (QDs) have been grown by Liu and co-workers, who found that Ag decoration led to a 6-fold increase in the sensing response toward 10–100 ppm NH_3 gas at room temperature [12]. Moreover, Wu et al. [13] found that for in-situ electrochemical activation through surface/interface modulation and enhancement of the catalytic performances of nanomaterials, novel bi-functional sandwich-like electrocatalysts of $FeCo_2O_4$@$FeCo_2S_4$@PPy or MCo_2O_4@MCo_2S_4@PPy can be used, which reveals that the bi-product interface can motivate more active sites than a single nanomaterials interface [13–16].

Some advantages of noble metal modified nanoparticles compared with pure precious metal catalysts are: the deposition time of nanoparticles is relatively small, the density of nanoparticles can be directed solely by the deposition time, and no precursor solutions need to be prepared.

An excellent example for the requirement of reliable gas sensors is *n*-butanol, which is a stimulating and narcotic volatile compound, used extensively as a solvent and extracting agent of organic synthesis intermediates [17]. However, exposure to *n*-butanol vapours has adverse health effects in humans, causing symptoms including dizziness, headaches, somnolence and dermatitis [7,17,18]. The traditional and most frequently used method for the detection of *n*-butanol is gas chromatography (GC) [17,19,20], which is a complicated, time-consuming and costly technique. The current trend of developing solid state gas sensors of low energy consumption, has led to the use of metal oxide semiconductors as good candidates to fabricate highly sensitive, selective and reliable *n*-butanol gas sensors [4,17,21].

Given that one of the important advantages to improve the highly selective sensitivity for certain specific gases and VOCs is the functionalization of the nanostructured semiconducting metal oxide surfaces with different types of noble metals [6], this study reports the fabrication of gas sensors for VOCs and H_2 using a titania/cupric oxide/cuprite (TiO_2/-CuO/Cu_2O/glass) heterostructure decorated with noble metal nanoparticles. To gain insight into the sensing mechanism, we also present calculations based on the density functional theory (DFT) of the ternary heterojunction $TiO_2(111)/CuO\left(\bar{1}11\right)/Cu_2O(111)$ decorated with Pd_7, Ag_7 and Ag_6Pt nanoparticles, where we have calculated the adsorption energies, structures and work functions after impregnation with the noble metal nanoclusters. Despite the lattice mismatch introduced by the deposition of the monoclinic $CuO\left(\bar{1}11\right)$ and $TiO_2(111)$ thin film overlayers on the $Cu_2O(111)$ substrate surface with hexagonal symmetry, this is a thermodynamically stable heterostructure [22,23]. The change of selectivity of the sensors is investigated by examining the binding energies and charge transfers for the interactions of molecular hydrogen (H_2), ethanol (C_2H_5OH) and *n*-butanol (*n*-C_4H_9OH) with the heteroepitaxial junctions functionalized by the noble metal nanoparticles.

This work demonstrates that the introduction of noble metal nanoparticles on the surface of TiO_2/CuO/Cu_2O presents a suitable route towards developing gas sensing devices with ultra-low energy consumption. The nanoscopic scale of the functionalisation also allows tuning, modulating and controlling the selectivity and response of these sensors, which can be used for practical applications requiring the discrimination between different VOCs and H_2 gas.

2. Material and methods

2.1. Experimental

Synthesis of the CuO-Cu_2O thin layers (20–60 nm of thickness) was achieved by sputtering a thin film of copper metal (Cu film with 20, 30, 40, 50 and 60 nm thicknesses) on top of a clean glass under vacuum conditions. The glass samples coated with the thin film of copper metal were thermally treated at 420 °C in an electrical furnace for 30 or 60 min under normal ambient conditions, because in the range of temperatures between 350 and 450 °C the mixed CuO/Cu_2O crystal phases are formed [22,24], which are well above the operating temperature (250 °C and 350 °C) used for our sensing measurements, ensuring that CuO is not transformed into the Cu_2O phase or vice versa during the sensing process. Next, titania (TiO_2) films of 20 nm thick were spray-deposited on top of the layers of the mixed copper oxide phases, thus preparing six additional sample sets. Afterwards, the samples of the TiO_2/CuO/Cu_2O heterostructure were treated in air at 420 °C for another 30 min (for the Cu20, Cu30, Cu40 samples) or 60 min (for the Cu50, Cu60 samples), depending on their thickness, before allowing them to cool down to room temperature. The next step comprised the sputtering of Au top-contacts on the surface of the fabricated TiO_2/-CuO/Cu_2O samples by means of a meander-shaped mask. The TiO_2/-CuO/Cu_2O thin films were decorated with Ag and AgPt alloy nanoparticles (Ag NP and AgPt NP) using a high vacuum deposition system (custom-made) with attached Gas Aggregation Source (GAS, Haberland type [25]). Details of the deposition of noble metal alloy nanoparticles can be found in our earlier work [7,26]. For the preparation of thin film composites with Pd NPs, a similar custom-constructed chamber for deposition under high vacuum and with attached Haberland-type GAS was used [9,11,27] following the technological approach developed by Lupan et al. [28].

A TiO_2/CuO/Cu_2O nanocomposite thin film, decorated with AgPt NPs, was investigated using X-ray photoelectron spectroscopy (XPS, Omicron Nano-Technology GmbH, Al, 240 W). The obtained XPS data were charge referenced with respect to aliphatic carbon C1s at 285.0 eV and analysed ("CasaXPS, version 2.3.16″) [9,11,27].

For the electrical studies, different bias voltages were applied to the functionalized samples and measurements were taken continuously and registered using a computer-controlled Keithley2400 sourcemeter using the LabView software (National Instruments). The gas response was determined as the ratio $(\frac{R_g-R_a}{R_a}\cdot 100\%)$, where R_g and R_a stand for the resistance of the device structures exposed to gas or air, accordingly [22,29].

The general technological flow process for the manufacture of the TiO_2/CuO/Cu_2O heterostructure-based sensor devices, which is represented in Fig. 1, consists of surface functionalization using Pd, Ag or AgPt nanoparticles. The inset of Fig. 1 represents a cross-section view of the multilayered devices comprising the Pd-, Ag- or AgPt-NPs/TiO_2/CuO/Cu_2O systems.

2.2. Computational details

We have used the Vienna Ab initio Simulation Package (VASP) [30–33] to carry out spin-polarised calculations within the usual Kohn-Sham (KS) implementation of the density functional theory (DFT). The generalised gradient approximation (GGA) was employed with the Perdew, Burke and Ernzerhof (PBE) functional for the exchange-correlation energy [34,35]. Long-range dispersion interactions were included using the semi-empirical method of Grimme, with the Becke-Johnson damping [D3-(BJ)] [36,37], which is required for the realistic simulation of the bulk and surface properties of several different materials [9,38–45]. The inner electron included up to the 3*s* level for Cu; 2*p* level for Ti; 4*f* level for Pt; 4*s* level for Pd and Ag; and 1*s* level for O, C and N, and were described by the projector augmented wave (PAW) method [46,47], whereas the electron of the H

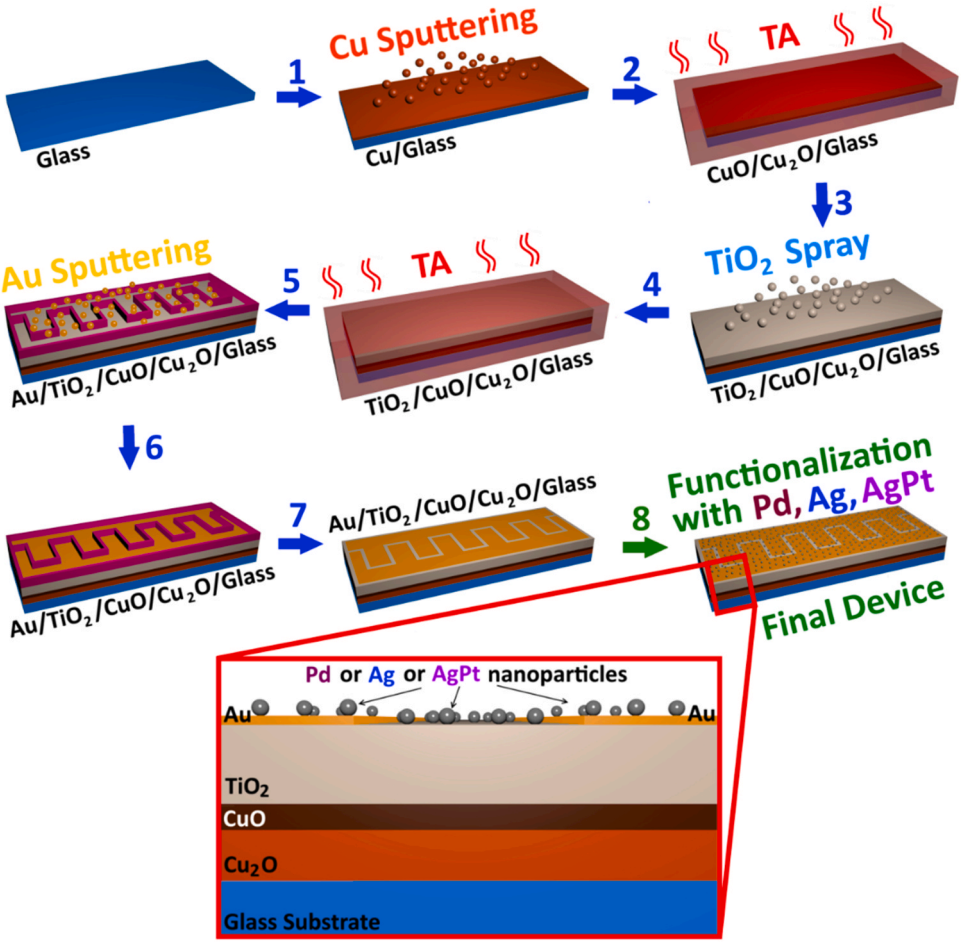

Fig. 1. The technological flowchart for the manufacture of the sensor device structures based on nanostructured layered films consisting of Pd, Ag or AgPt NPs on top of the $TiO_2/CuO/Cu_2O$ heterostructure (Final device structure). Cross-section view of a device based on Pd, Ag or AgPt NPs on top of the $TiO_2/CuO/Cu_2O$ -based sensor in the inset.

atom was treated as valence. The valence states were expanded in a periodic plane-wave basis set with a cut off at 400 eV for the kinetic energy. An energy threshold defining self-consistency of the electron density was set at 10^{-5} eV. An efficient conjugate-gradients technique based on the Newton line optimiser [48,49] was used for the relaxation of the geometries, which reached the ground state when the Hellmann-Feynman forces on all atoms were smaller than 0.01 eV $Å^{-1}$. We have used the Hubbard approximation [50] in the form of the Dudarev et al. [51] scheme to improve the description of localised *d* states in this type of system, where the standard GGA functionals fail [52]. The values for the on-site Coulomb interaction term in this study were $U_{eff} = 4.0$ eV for Cu and 4.4 eV for Ti [22,23, 53–57]. However, no Hubbard Hamiltonian was applied to the *d* states of the noble metal NPs, as they are already delocalised given the electron conducting properties of these materials [58,59]. These criteria allowed convergence of the total electronic energy to within 1 meV $atom^{-1}$.

The electronic integrations of the face-centred cubic (*fcc*) transition metal phases were calculated in the reciprocal space using their primitive unit cells and a Γ-centred Monkhorst-Pack (MP) sampling grid [60] containing $17 \times 17 \times 17$ *k*-points, which was sufficient to simulate correctly their conducting electronic properties [58,59]. The nanoparticle -functionalised $TiO_2(111)/CuO\left(\bar{1}11\right)/Cu_2O(111)$ heterostructure was simulated using a Γ-centred MP mesh [60] of $5 \times 5 \times 1$ *k*-points, in line with previous works [22,23]. The isolated molecules were modelled in a cell with broken symmetry and dimensions of $20 \times 21 \times 22$ $Å^3$, considering only the Γ point of the Brillouin zone. The electronic partial occupancies of the isolated molecules were determined using the Gaussian smearing method with a smearing width of 0.05 eV. The method of Methfessel-Paxton order 1 with a sigma value of $\sigma = 0.2$ eV was applied to the *fcc* metal phases [61], which ensured a negligible variational quantity, i.e. electronic entropy [62]. Moreover, the tetrahedron method with Blöchl corrections [63] was used for the calculation of the electronic and magnetic properties and to obtain very accurate total energies for the nanoparticle functionalised heteroepitaxial junctions before and after molecular adsorption of the gases.

3. Results and discussion

3.1. Morphological evolutions and composition analysis

Scanning electron microscope (SEM) images are presented in Fig. 2 for the mixed copper oxide CuO/Cu_2O substrate coated with a TiO_2 layer and functionalised with the Pd, Ag and AgPt noble metal nanoparticles. The surface of the $TiO_2/CuO/Cu_2O$ material is covered with nanoclusters of 5–15 nm in diameter, which are forming uniformly interconnected nano-crystallites, which is favourable for sensor device applications. The SEM images of the CuO/Cu_2O, $TiO_2/CuO/Cu_2O$ and $AgPt/TiO_2/CuO/Cu_2O$ samples are shown in Figs. S1. To better understand the structures, the SEM images at high and low magnification are represented in Figs. S2 and S3 in the Supporting Information.

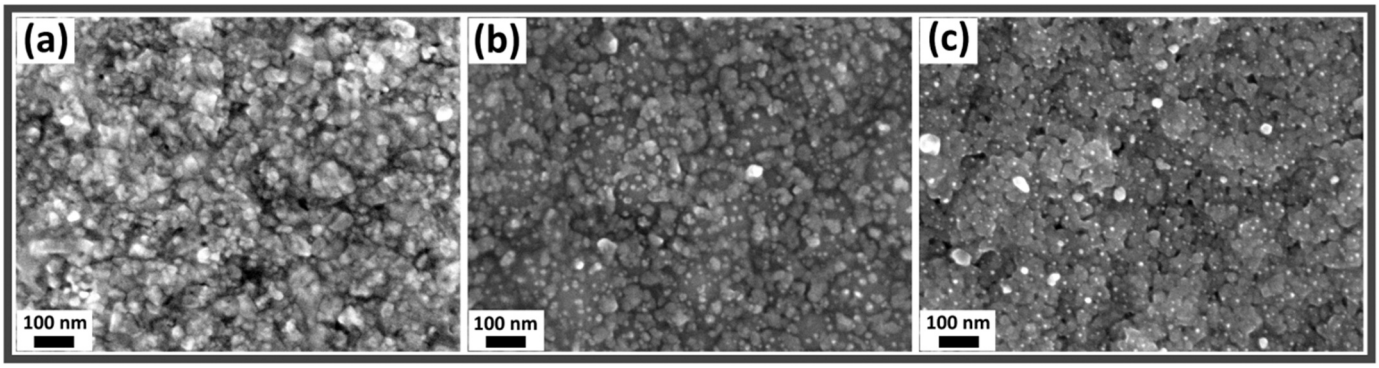

Fig. 2. Higher magnification of SEM images of interconnected TiO_2/CuO/Cu_2O nano-crystallite samples covered with: (a) Pd nanoparticles, with CuO/Cu_2O thickness of 20 nm (Cu20); (b) Ag nanoparticles, with CuO/Cu_2O thickness of 60 nm (Cu60); (c) AgPt nanoparticles, with CuO/Cu_2O thickness of 60 nm (Cu60)). Noble metal nanoclusters have 5–15 nm in diameter.

3.2. X-ray photoelectron spectroscopy, micro-Raman and UV-Visible-NIR spectroscopy characterisation of CuO/Cu_2O and TiO_2/CuO/Cu_2O nanocomposite

The X-ray photoelectron spectra (XPS) of the TiO_2/CuO/Cu_2O nanocomposite decorated with AgPt NPs are shown in Fig. 3. Cu, O, Ti, Na and C elements were detected in both the nanocomposite as well as in the TiO_2/CuO/Cu_2O reference thin film, see the overview spectra in Fig. 3a. The presence of Cu, O and Ti originates from the TiO_2/CuO/Cu_2O base layer, although the signal from carbon is due to contamination of the top surface with C from the atmosphere, e.g. from carbohydrates [9,11,27]. The observation of the signal corresponding to Na is due to diffusion from the glass substrates, which were used for the deposition of the sensor structures [7,64,65]. Such peaks were not detected from samples deposited on quartz substrates (not shown here).

Fig. 3b depicts the high-resolution spectra of the Cu-2p, Ti-2p, Ag-3d and Pt-4d lines. A closer look at the Cu-2p line reveals clear satellite peaks for both the Cu-2$p_{3/2}$ and Cu-2$p_{1/2}$ lines, which are relocated to

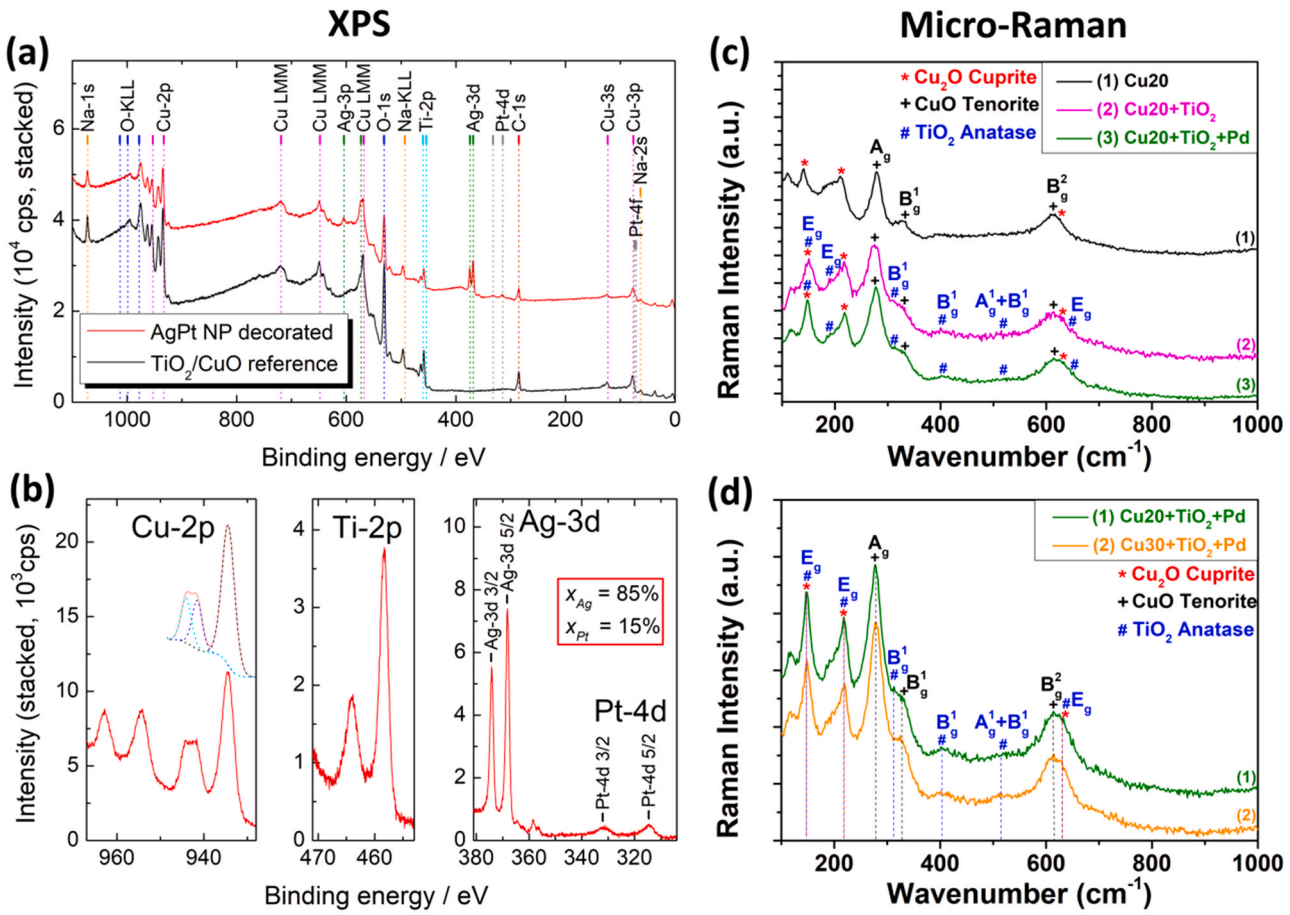

Fig. 3. X-ray photoelectron spectra (XPS) of: (a) a AgPt/TiO_2/CuO/Cu_2O (red line) nanocomposite and an undecorated TiO_2/CuO/Cu_2O thin film (black line); (b) spectra at higher resolution for Cu-2p and Ti-2p lines as well as spectra for Ag-3d and Pt-4d lines. Micro-Raman spectra for: (c) the surface functionalized TiO_2/CuO/Cu_2O and Pd/TiO_2/CuO/Cu_2O samples with CuO/Cu_2O thickness of 20 nm (Cu20) after being thermally treated at 420 °C for 30 min in ambient; (d) Pd/TiO_2/CuO/Cu_2O with CuO/Cu_2O thicknesses of 20 nm (Cu20) and 30 nm (Cu30), respectively.

higher binding energies. The Cu-$2p_{3/2}$ line, as well as the corresponding satellites, were assigned to the nanocomposite – see deconvolution of $2p_{3/2}$ with satellite peaks into 3 subpeaks. The observed satellite peaks are generally regarded as a signature for the occurrence of the CuO/Cu_2O heterojunction with CuO exposed at the surface [8,9]. Accordingly, the signal from copper in the spectrum can be assigned to the existence of CuO/Cu_2O in the base layer.

A Ti-$2p_{3/2}$ peak in the range 459.6–458.0 eV is usually assigned to Ti^{4+} in TiO_2. The evaluation of high resolution Ti-2p XPS binding energies reveals that the Ti-$2p_{3/2}$ line is positioned around 458.3 eV. The peak positions of Ti-$2p_{3/2}$ and Ti-$2p_{1/2}$ and their separation of 5.6 eV indicate the presence of Ti in the form of TiO_2 in the base layer [66,67].

Ag and Pt were detected alongside Cu, Ti, O and C in the TiO_2/CuO/Cu_2O nanocomposite decorated using the AgPt NPs. Spectra at higher resolution of the Ag-3d and Pt-4d lines were recorded in order to evaluate the composition of the AgPt NPs. We chose the Pt-4d lines for quantification due to the overlap of Pt-4f with intensive Cu-3p lines. In the case of the nanocomposite, the quantification of the AgPt NPs yields a platinum content of roughly 15 at% within the nanoparticles. A detailed investigation of AgPt NPs can be found in our earlier works [7,11].

In addition to the functionalisation of the TiO_2/CuO/Cu_2O nanocomposite with AgPt NPs, we also used Pd nanoparticles [28] to prepare the decorated sensors in the context of this work. The respective overview and high-resolution spectra corresponding to the TiO_2/CuO structures with and without decoration by Pd NPs are shown in Fig. S4 (Supporting Information). In general, the spectra of the AgPt nanoparticle- and Pd nanoparticle-decorated sensors show strong similarities and mostly differ in the signals corresponding to the elemental Ag, Pt or Pd. The observation of the Pd-3d lines with peaks around 335.8 eV (Pd-$3d_{5/2}$) and 341.0 eV (Pd-$3d_{3/2}$) indicates the successful decoration of the sensor structure by Pd nanoparticles [28].

The micro-Raman spectra of the CuO/Cu_2O, TiO_2/CuO/Cu_2O and Pd/TiO_2/CuO/Cu_2O nanocomposites, which were investigated at room temperature in the range 100–1000 cm^{-1}, are shown in Fig. 3c and d. The presence of metallic Cu and Pd could not be ascertained in these materials, due to the instrumental limitations related to the measurement of their dielectric constants, which possess negative real and imaginary positive components exhibited in the surface plasmon resonance (SPR) experiments [68,69]. In the case of the metal nanoclusters, the local SPRs are pledged for the field improvement, which undergo surface-enhanced processes [68,69], that are only observed when using surface-enhanced Raman spectroscopy. Only phonon frequencies of the crystalline Cu_2O, CuO and TiO_2 layers are observed with our experimental set-up, as the group theory indicates that the Raman response is a function of the space group symmetry of the crystal [70].

Fig. S5 illustrate the Ultraviolet, Visible and Near InfraRed (UV-Vis-NIR) absorption spectra for the Pd/TiO_2/CuO/Cu_2O heterostructures, which confirm the energy structures and optical properties of this transparent semiconducting oxide. The Tauc plots for the Pd/TiO_2/CuO/Cu_2O heterostructures, presented in Fig. S6, reveal a bandgap that widens with the reduction of the nanoparticle size from 30 to 10 nm. As expected, the absorption edge of 2.04 eV for the 20 nm sample is equal to the value published for bulk Cu_2O [71–74].

3.3. Gas sensing properties

Heterostructures formed by *p-n* semiconductors, especially those functionalized with noble metals have a high catalytic activity and can be used to enhance the surface reactions of chemical sensing materials [7,75]. It is known that the functionalization of oxides (such as ZnO, SnO_2, TiO_2, Cu_2O and Fe_2O_3) with different noble metals or their alloys improves significantly their sensing performance. In this section the sensing properties of the TiO_2/CuO/Cu_2O heterostructure functionalized with the Pd, Ag or AgPt NPs will be discussed.

3.3.1. Gas sensing properties of Pd/TiO_2/CuO/Cu_2O heterostructures

The gas sensing characteristics of the TiO_2/CuO/Cu_2O samples with CuO/Cu_2O thickness of 20 nm (Cu20) functionalized using Pd NPs (Pd-NPs/TiO_2/CuO/Cu_2O) were investigated towards different volatile organic compounds and hydrogen. Our main aim is to show experimentally that Pd-functionalization of such structures significantly increases the response and selectivity to hydrogen gas, even at low operating temperature. We also intend to demonstrate that it is possible to lower the energy consumption during operation and tune the reactivity toward H_2 of the TiO_2/CuO/Cu_2O heterojunction sensors through functionalization by Pd nanoparticles.

Fig. 4a shows the response versus operating temperature to hydrogen, *n*-butanol, 2-propanol, ethanol, acetone, ammonia and CH_4 by the TiO_2/CuO/Cu_2O samples after surface functionalization with the Pd-NPs (for a CuO/Cu_2O specimen of 20 nm of thickness labelled as Cu20 set sample), where we observe a high and selective response to H_2 at all working temperatures. The responses are ~405%, ~487%, ~543% and ~371% at the operating temperatures of 150 °C, 200 °C, 250 °C and 300 °C, respectively. The optimal operating temperature was found within the range 200–250 °C. Fig. 4b shows the dynamic hydrogen response of the Pd-NPs/TiO_2/CuO/Cu_2O (Cu20) samples at different operating temperatures. The calculated response times (τ_r = 18.7, 20.4, 12.8 and 12.4 s) and recovery times (t_d = (>50), 36.3, 10.6 and 4.2 s) are relatively small at the operating temperatures of 150 °C, 200 °C, 250 °C and 300 °C, respectively, see Fig. S7a. The dynamic response to different gases (hydrogen, *n*-butanol, 2-propanol, ethanol, acetone, ammonia and CH_4) of Pd-NPs/TiO_2/CuO/Cu_2O with CuO/Cu_2O thickness of 20 nm (Cu20) at an operating temperature of 250 °C can be seen in Fig. S7b. Fig. 4c shows that the current increases with the operating temperature for the Pd/TiO_2/CuO/Cu_2O material. Fig. 4d shows the dynamic response to different hydrogen concentrations (5, 10, 50, 100, 500 and 1000 ppm) of the functionalized Pd/TiO_2/CuO/Cu_2O (Cu20) samples, where a fairly high response of ~88% is registered at 5 ppm. The dynamic response to H_2 gas with concentrations of 5 and 50 ppm is presented in Fig. S8.

Fig. S9a presents the response to hydrogen, *n*-butanol, 2-propanol, ethanol, acetone and ammonia of the Pd/TiO_2/CuO/Cu_2O (for a substrate with CuO/Cu_2O thickness of 30 nm, referred as Cu30) samples, which possess the highest response towards H_2 gas (>550%). Fig. S9c displays the dynamic response to hydrogen of the Pd/TiO_2/CuO/Cu_2O (Cu30) samples at various OPTs and Fig. S9d illustrates the dynamic response to hydrogen gas with three consecutive pulses at the operating temperatures 300 °C. These samples clearly show superior sensing performances, which can be of major practical interest in device applications.

3.3.2. Gas sensing properties of Ag/TiO_2/CuO/Cu_2O

Next, the surface functionalization with the Ag nanoparticles of the TiO_2/CuO/Cu_2O samples (CuO/Cu_2O with thickness of 60 nm (Cu60)) was realised to tune the response to VOCs, namely to change the selectivity from ethanol (in the case of the CuO/Cu_2O samples) to *n*-butanol.

Fig. 5a shows the response to several gases versus the OPTs of the surface functionalized Ag/TiO_2/CuO/Cu_2O (Cu60) samples (CuO/Cu_2O with thickness of 60 nm). We observe that, at the low operating temperatures of 200 °C, the sample has *n*-type conductivity and shows sensing capabilities only towards 2-propanol and ethanol, because the electrical resistivity decreases after the molecular interactions. At the working temperatures OPTs of 250 °C, 300 °C and 350 °C, the sample already has *p*-type conductivity and is therefore selective to *n*-butanol, where the responses are ~54%, ~200%, and ~163%, respectively. This phenomenon is dictated by the composition of the sample, which changes the surface activity and reaction products [7,22,23], by band bending and formation of electron depletion or space charge layer in the conduction band, that either decreases or increases the conductivity of the active materials [76]. The lower operating temperature does not

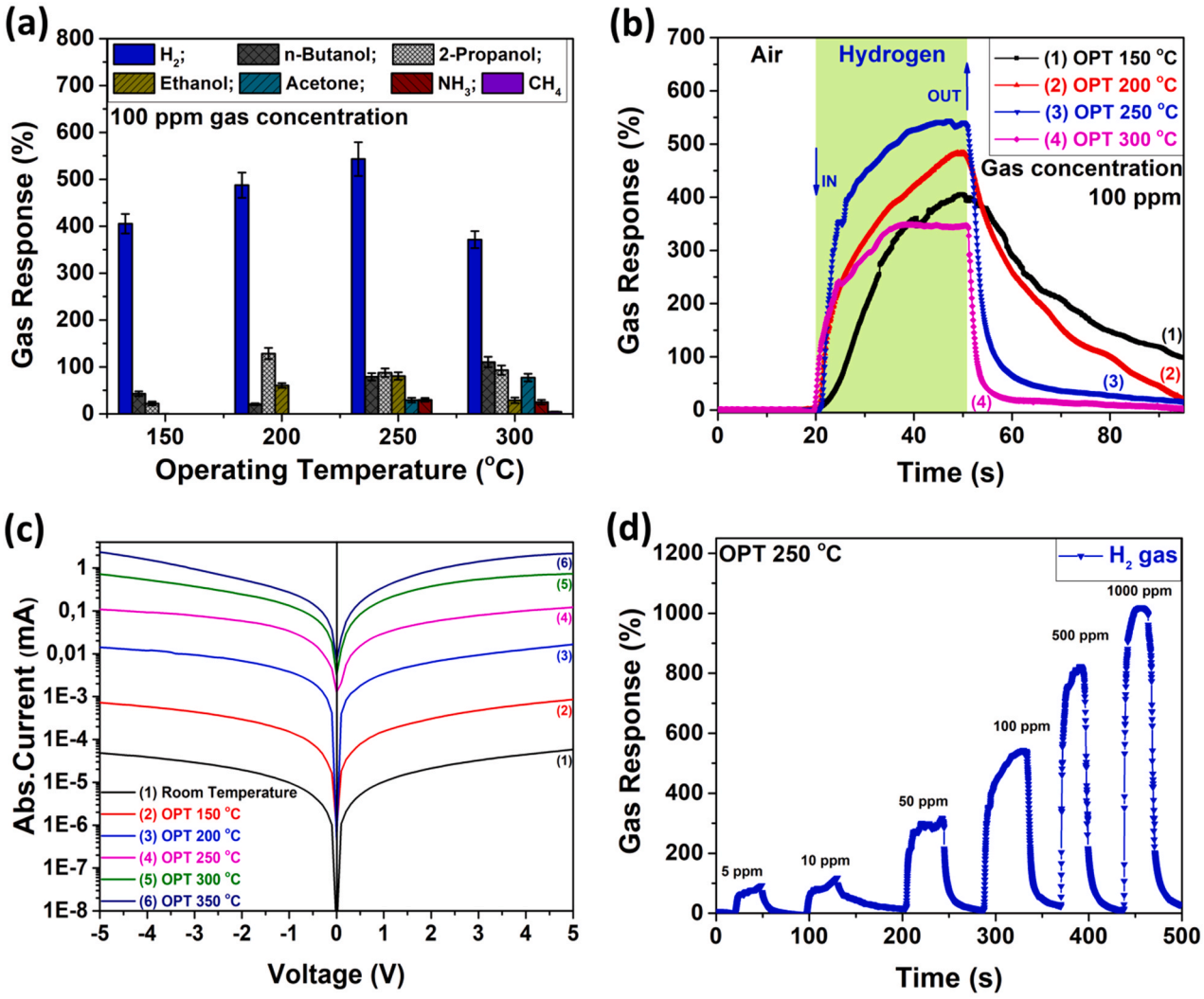

Fig. 4. (a) Gas response towards different compounds (hydrogen, *n*-butanol, 2-propanol, ethanol, acetone, ammonia and CH_4) of the Pd-functionalized TiO_2/CuO/Cu_2O samples with CuO/Cu_2O thickness of 20 nm (Cu20) at different operating temperatures (OPT); (b) Dynamic response to hydrogen of the Pd/TiO_2/CuO/Cu_2O samples with CuO/Cu_2O thickness of 20 nm (Cu20) measured at several OPTs; (c) The I-V current-voltage characteristics of the Pd/TiO_2/CuO/Cu_2O samples with CuO/Cu_2O thickness of 20 nm (Cu20) at different OPT; (d) Dynamic response to different concentrations of hydrogen (5, 10, 50, 100, 500 and 1000 ppm) of the Pd/TiO_2/CuO/Cu_2O samples with CuO/Cu_2O thickness of 20 nm (Cu20) (applied bias voltage of 250 mV).

influence the depletion layer of electrons in TiO_2, whereas the CuO/-Cu_2O layer has a higher resistance, forcing currents flowing through the TiO_2 layer which is an *n*-type semiconductor. However, at higher operating temperatures the depletion layer of electrons in TiO_2 and the accumulation layer of holes in CuO/Cu_2O are also affected. As a result, the CuO/Cu_2O layer impacts the sensing mechanism, which increases the heterojunction resistance to the application of the target gas [77]. Fig. 5b shows the dynamic response towards hydrogen, *n*-butanol, 2-propanol, ethanol and acetone for the Ag/TiO_2/CuO/Cu_2O (Cu60) samples at the optimal OPT of 300 °C.

Fig. 5c shows the current-voltage performance of the Ag/TiO_2/CuO/Cu_2O (Cu60) samples, where the conductance increases with the operating temperature in the tested range. Fig. 5d displays the dynamic response to 5, 10, 50, 100, 500 and 1000 ppm of *n*-butanol for the Ag/TiO_2/CuO/Cu_2O (Cu60) samples, demonstrating that a response of about 31% is registered even for the lowest concentration of this gas. The dynamic response to 5, 50 and 100 ppm of *n*-butanol of the Ag/TiO_2/CuO/Cu_2O samples with CuO/Cu_2O thickness of 60 nm (Cu60) at the operating temperature of 300 °C is presented in Fig. S10. Fig. 5e displays the dynamic response to 100 ppm of *n*-butanol and consecutively 2-propanol, acetone, ethanol in air, of Ag/TiO_2/CuO/Cu_2O samples. Fig. 5f displays the dynamic response to 100 ppm of *n*-butanol and mixtures of alcohols in air, with and without *n*-butanol vapours, with 1000 ppm of Ag/TiO_2/CuO/Cu_2O samples.

3.3.3. *Gas sensing properties of AgPt/TiO_2/CuO/Cu_2O*

Next, the response to different compounds by the AgPt/TiO_2/CuO/Cu_2O (Cu60) samples were studied at various working temperatures to investigate whether we can tune the selectivity by means of changing the composition of the NPs.

Fig. 6a shows the response to hydrogen, *n*-butanol, 2-propanol, ethanol and acetone versus the OPT for the surface-functionalized AgPt/TiO_2/CuO/Cu_2O samples with CuO/Cu_2O thickness of 60 nm (Cu60). At the OPT of 250 °C, 300 °C and 350 °C, the sample is selective to *n*-butanol and the responses are ~78%, ~118%, and ~216%, respectively, suggesting that the optimal operating temperature is therefore 350 °C. Fig. 6b illustrate the dynamic response to hydrogen, *n*-butanol, 2-propanol, ethanol and acetone of the AgPt/TiO_2/CuO/Cu_2O (Cu60) samples at the operating temperatures of 350 °C. Fig. 6c illustrate the current-voltage characteristics of AgPt/TiO_2/CuO/Cu_2O (Cu60) samples, where we observe that the conductance increases with the operating temperature. Fig. 6d shows the dynamic response to 5, 10, 50, 100, 500 and 1000 ppm of *n*-butanol for the Cu60 AgPt/TiO_2/CuO/

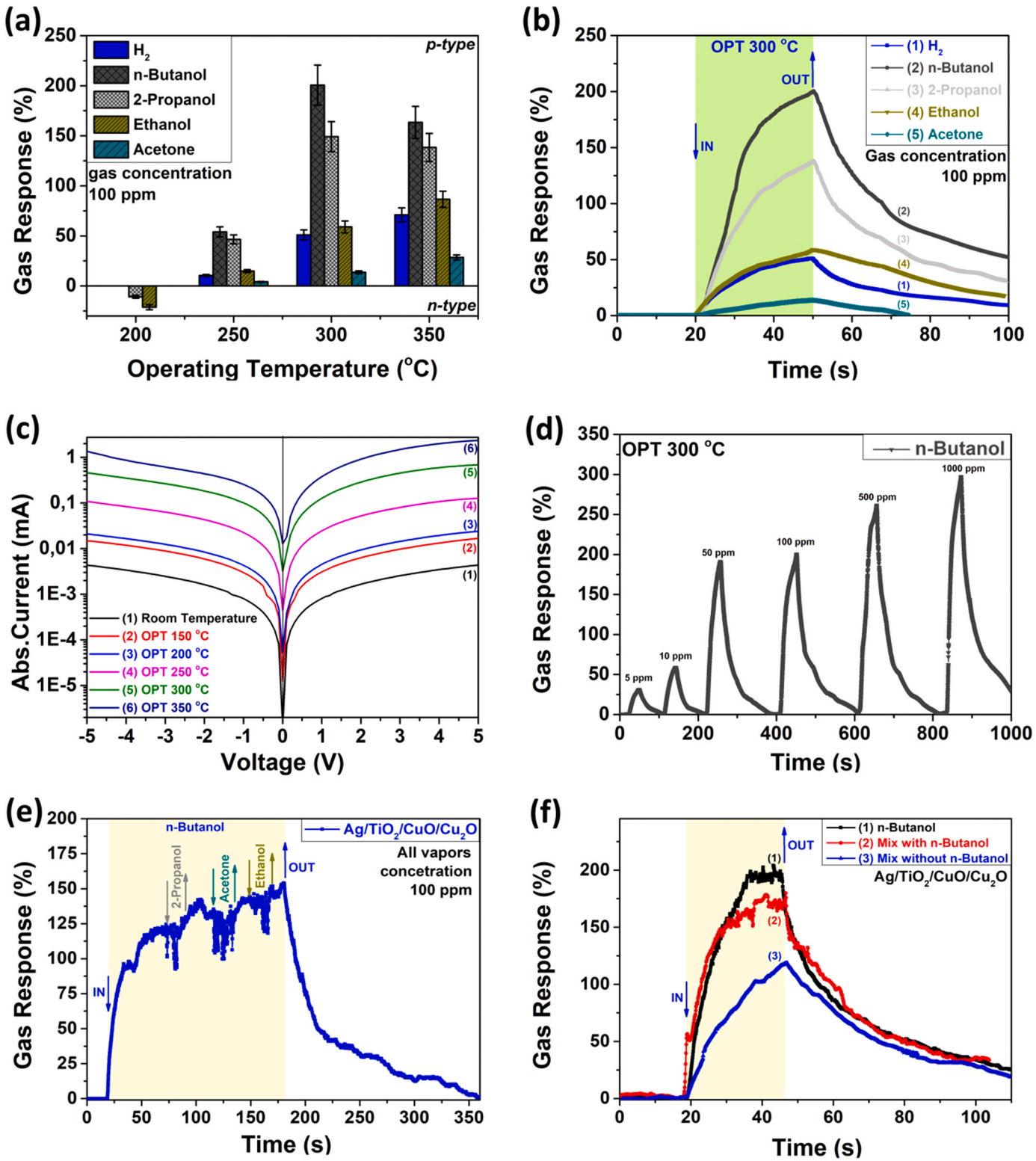

Fig. 5. (a) Gas response towards hydrogen, *n*-butanol, 2-propanol, ethanol and acetone for the $TiO_2/CuO/Cu_2O$ samples after surface functionalization with Ag-nanoparticles (CuO/Cu_2O with thickness of 60 nm (Cu60)); (b) Dynamic response to different compounds (hydrogen, *n*-butanol, 2-propanol, ethanol and acetone) of the $Ag/TiO_2/CuO/Cu_2O$ (Cu60) samples at the operating temperature of 300 °C. (c) The current – voltage behaviour of the $Ag/TiO_2/CuO/Cu_2O$ (Cu60) samples at different operating temperatures; (d) Dynamic response to various concentrations of *n*-butanol (5, 10, 50, 100, 500 and 1000 ppm) of the $Ag/TiO_2/CuO/Cu_2O$ (Cu60) samples (applied bias voltage 27.5 mV). (e) Dynamic response to 100 ppm of *n*-butanol and consecutively 2-propanol, acetone, ethanol in air of $Ag/TiO_2/CuO/Cu_2O$ samples. (f) Dynamic response to 100 ppm of *n*-butanol and mixture of alcohols in air, with and without *n*-butanol vapours with 1000 ppm of $Ag/TiO_2/CuO/Cu_2O$ samples.

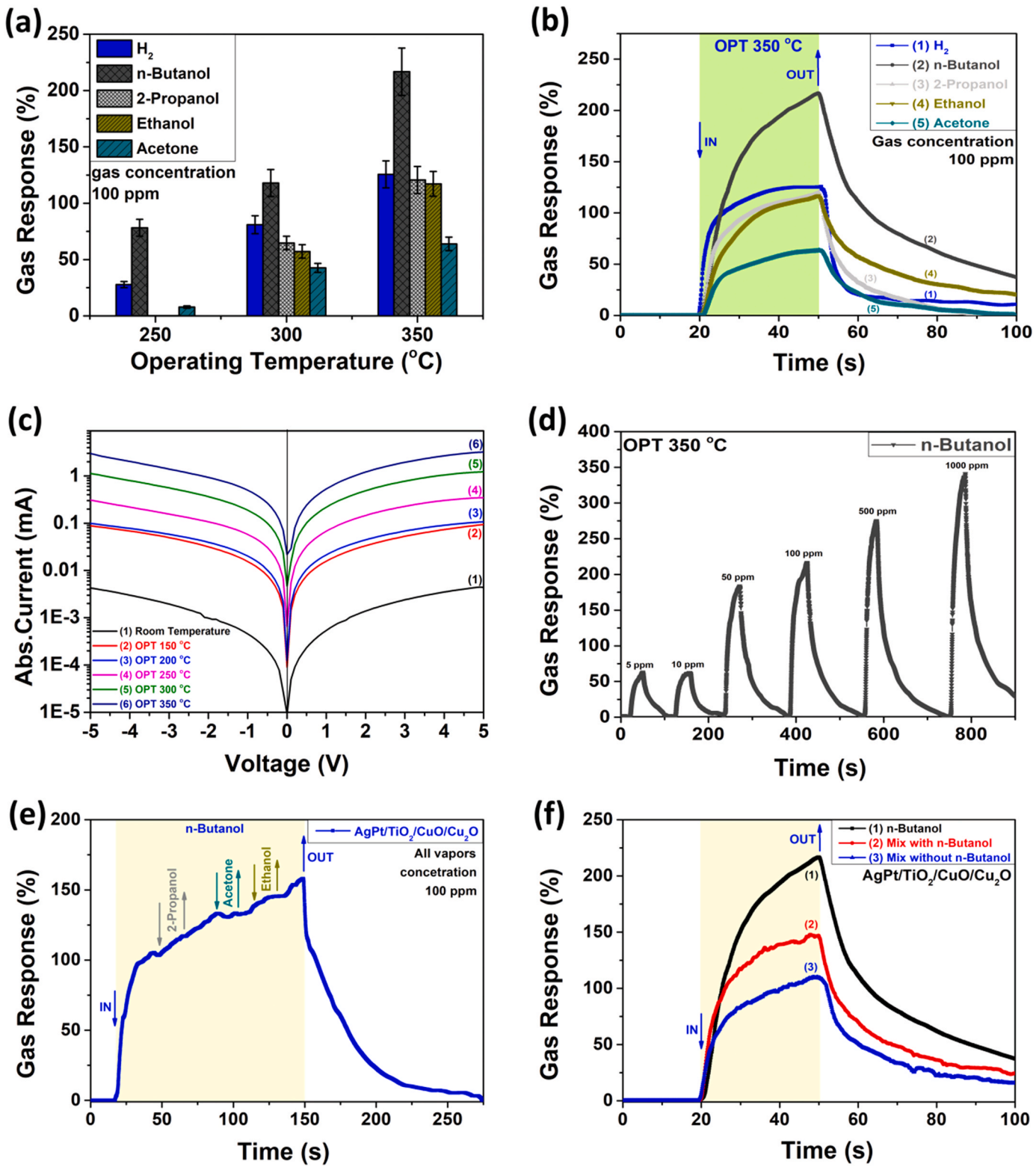

Fig. 6. (a) Gas response to different gases and volatiles (hydrogen, *n*-butanol, 2-propanol, ethanol and acetone) of the AgPt-NPs surface functionalized TiO_2/CuO/Cu_2O samples with CuO/Cu_2O thickness of 60 nm (Cu60); (b) Dynamic response to hydrogen, *n*-butanol, 2-propanol, ethanol and acetone for AgPt/TiO_2/CuO/Cu_2O (Cu60) samples at the operating temperature of 350 °C. (c) Current-voltage characteristic of the AgPt/TiO_2/CuO/Cu_2O (Cu60) samples at different operating temperatures; (d) Dynamic response to 5, 10, 50, 100, 500 and 1000 ppm of *n*-butanol of AgPt/TiO_2/CuO/Cu_2O (Cu60) samples (applied bias voltage 9.5 mV). (e) Dynamic response to 100 ppm of *n*-butanol and consecutively 2-propanol, acetone, ethanol in air of AgPt/TiO_2/CuO/Cu_2O samples. (f) Dynamic response to 100 ppm of *n*-butanol and mixtures of alcohols in air with and without *n*-butanol vapours with 1000 ppm of AgPt/TiO_2/CuO/Cu_2O samples.

Cu_2O samples with CuO/Cu_2O thickness of 60 nm, where a response of ~63% is registered for 5 ppm of *n*-butanol. Fig. 6e displays the dynamic response to 100 ppm of *n*-butanol and consecutively 2-propanol, acetone, ethanol in air of $AgPt/TiO_2/CuO/Cu_2O$ samples. Fig. 6f displays the dynamic response to 100 ppm of *n*-butanol and mixtures of alcohols in air with and without *n*-butanol vapours with 100 ppm of $AgPt/TiO_2/CuO/Cu_2O$ samples. The dynamic response of the $AgPt/TiO_2/CuO/Cu_2O$ samples (Cu60) to 5, 50 and 100 ppm of *n*-butanol at the OPT of 350 °C is presented in Fig. S11. Thus, chemical sensitisation facilitates the adsorption of certain gas molecules on the metal NP surface, thus inducing more interactions with pre-absorbed oxygen species, facilitating relevant chemical reactions, the charge transfer, increase the electrocatalytically active surface area and therefore an improved gas detection performance [5,6].

3.3.4. *Comparison of the gas sensing properties and energy consumption of the heterostructures*

In this section, we compare the gas responses for the $TiO_2/CuO/Cu_2O$ heterostructures functionalized with the different types of NPs-, as we aim to show the possibility of controlling their selectivity by using the technological approach developed in this work.

Fig. 7a shows the gas response to hydrogen, *n*-butanol, 2-propanol, ethanol and acetone for the $Pd/TiO_2/CuO/Cu_2O$, $Ag/TiO_2/CuO/Cu_2O$, and $AgPt/TiO_2/CuO/Cu_2O$ samples. The samples functionalized with Pd nanoparticles are the most sensitive to hydrogen, whereas the samples functionalized using the Ag and AgPt nanoparticles experience a change of selectivity and are the most sensitive to butanol.

Fig. 7b represents the dependence of the power consumption and of the response to 100 ppm of H_2 gas versus the applied bias voltage for the $Pd/TiO_2/CuO/Cu_2O$ samples with CuO/Cu_2O thickness of 20 nm (Cu20). According to the figure, both the power consumption and the response to the H_2 gas decreases when the applied voltage is decreased. However, we also observed that for an applied bias voltage of 10 mV the response increased. The power consumption obtained is ~270, ~140, ~4.1 and ~0.19 nW, and the responses are ~588%, ~404%, ~310% and ~390%, at the applied bias voltages of 250, 100, 50 and 10 mV, respectively. The response to different gases versus the applied bias voltage for the $Pd/TiO_2/CuO/Cu_2O$ samples with CuO/Cu_2O thickness of 20 nm (Cu20) is represented in Fig. S12. The dependence on the power consumption and the response to 100 ppm of *n*-butanol vapours versus applied bias voltage for $Ag/TiO_2/CuO/Cu_2O$ with CuO/Cu_2O thickness of 60 nm are represented in Fig. 7c, where it can be seen that the obtained power consumption is ~170, ~56, ~23.5 and ~17.6 nW, and the respective responses are ~104%, ~121%, ~200% and ~210%, at the applied bias voltages of 85, 50, 30 and 27.5 mV, respectively. For the $AgPt/TiO_2/CuO/Cu_2O$ samples with CuO/Cu_2O thickness of 60 nm (Cu60), the power consumption is ~10.6, ~8.4 and ~7.2 nW, and the responses are ~162%, ~180% and ~216% to 100 ppm of *n*-butanol vapours at the applied bias voltages of 12.5, 11.0 and 9.5 mV, respectively, shown in Fig. 7d, where it can be seen that the obtained power consumption is ~10.6 nW, ~8.4 nW and ~7.2 nW, and the respective responses are ~162%, ~180% and ~216%, at the applied voltages of 12.5 mV, 11.0 mV and 9.5 mV, respectively. The dependence on the power consumption versus the applied bias voltage is represented in Fig. S13 for the $TiO_2/CuO/Cu_2O$ samples with CuO/Cu_2O thickness of 20 nm (Cu20) decorated with Pd or Ag or AgPt NPs.

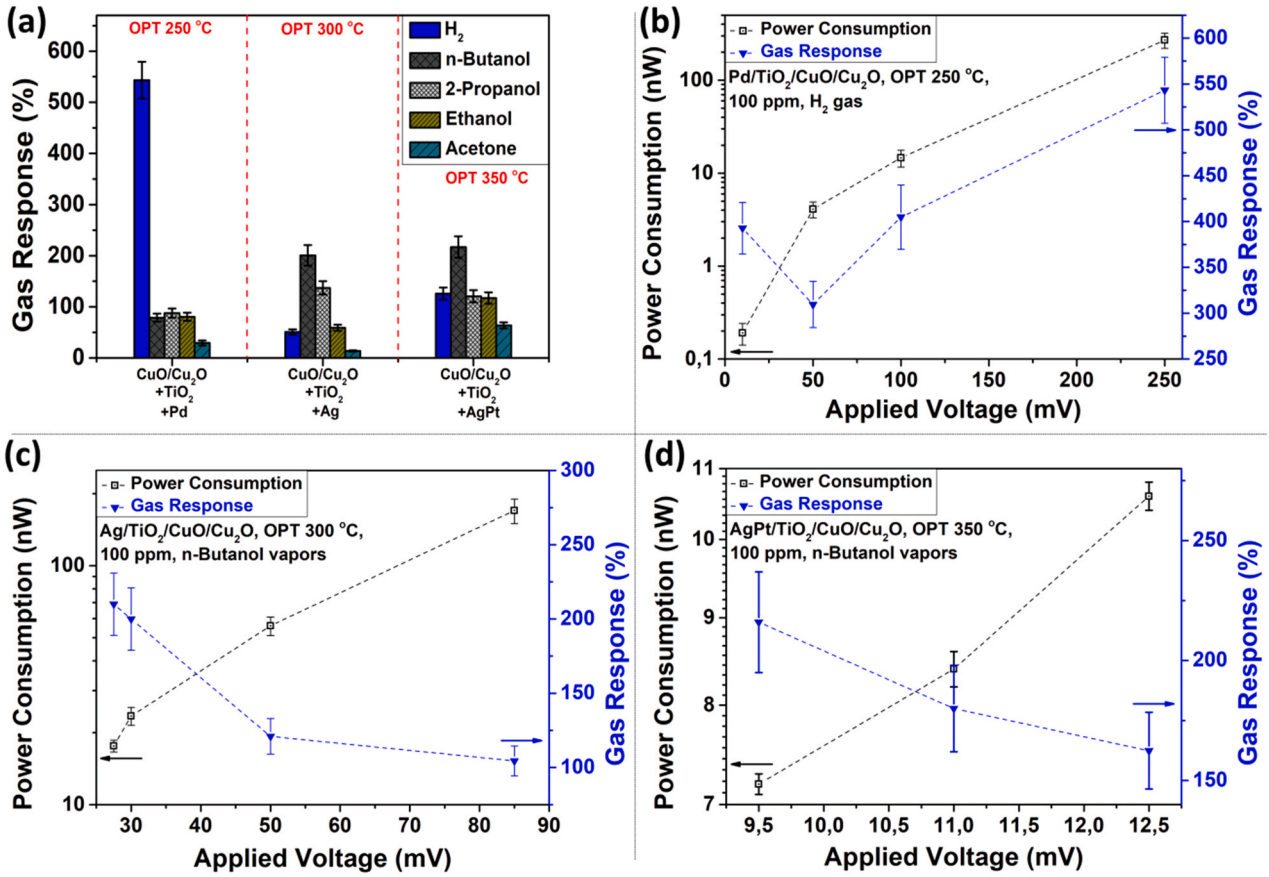

Fig. 7. (a) Gas response to different compounds (hydrogen, *n*-butanol, 2-propanol, ethanol and acetone) of the $Pd/TiO_2/CuO/Cu_2O$, $Ag/TiO_2/CuO/Cu_2O$, and $AgPt/TiO_2/CuO/Cu_2O$ samples. Dependence of the power consumption and of the gas versus the applied bias voltage for: (b) $Pd/TiO_2/CuO/Cu_2O$ (with CuO/Cu_2O thickness of 20 nm (Cu20)), (c) $Ag/TiO_2/CuO/Cu_2O$ (with CuO/Cu_2O thickness of 60 nm (Cu60)), and (d) $AgPt/TiO_2/CuO/Cu_2O$ (with CuO/Cu_2O thickness of 60 nm (Cu60)).

The proposed gas sensing mechanism for our heterostructures after functionalization with noble metal nanoparticles is described in Text S1 (Supporting Information).

3.4. Deposition of nanoparticles: computational results

We have simulated the modification of the ternary $TiO_2(111)/CuO\left(\bar{1}11\right)/Cu_2O(111)$ heterostructure by adsorbing Pd_7, Ag_7 and Ag_6Pt nanoparticles, see Fig. 8, to subsequently assess their selectivity and sensitivity towards the detection of hydrogen (H_2), ethanol (C_2H_5OH) and *n*-butanol (C_4H_9OH) vapours. The purpose of these simulations is to assist the interpretation of the trends of the gas response detected in the experiments for our ternary heterojunctions functionalised using noble metal nanoparticles.

The scanning tunnelling microscopy images (STM), shown in Fig. 8d-f, were simulated using the HIVE code [78], which is based on the theory developed by Tersoff and Hamann [79]. The brightest spots resolved for the surface of the nanoparticle-functionalised ternary $TiO_2(111)/CuO\left(\bar{1}11\right)/Cu_2O(111)$ material correspond to the noble metal clusters. Fig. 8d clearly shows the almost perfect 5-fold symmetry of the Pd_7 NP, which is only broken by the Pd atom located away from the nanoparticle axis. Following deposition, the Ag_7 cluster splits into conjoined twin particles, each containing three metal atoms, connected by a bridge comprising one Ag atom, as shown in Fig. 8e. Fig. 8f illustrates that replacing the axial and exposed Ag atom by Pt has a cohesive effect in the conjoined twin particles, which reattach in a pentagon shape, although still more distorted than Pd_7. We discuss changes in the interfacial energy and work function after NP functionalisation of $TiO_2(111)/CuO\left(\bar{1}11\right)/Cu_2O(111)$ in the Supporting Information. The adsorption energies of the noble metal NPs, charge transfers and their magnetic moments are also analysed in the Text S2 (Supporting Information).

The work function of the ternary heterojunction suffers a reduction of approximately 37% from its initial large value of $\Phi = 7.454$ eV, after decoration by the noble metal nanoparticles, as listed in Table S1 and described in the Text S3 (Supporting Information). The lower work function values calculated for the hetero-devices after surface functionalisation explain their enhanced chemical reactivity, compared to the material before deposition of the metal nanoclusters. Our simulated work functions show small differences of up to 0.14 eV, suggesting that the composition of the nanoparticles can be used to fine-tune the application of the nano-composite materials as chemical sensors.

3.5. Adsorption of molecules: computational results

Here, we have modelled the surface chemistry of the ternary heteroepitaxial junction materials decorated with nanoparticles of noble metals or their alloys.

The binding energies for the interaction between the adsorbate molecules and the $TiO_2(111)/CuO\left(\bar{1}11\right)/Cu_2O(111)$ layered material functionalised with the Pd_7 nanoparticle, show a preference for H_2, releasing −1.494 eV upon interaction, see Table S2. Table S2 also lists

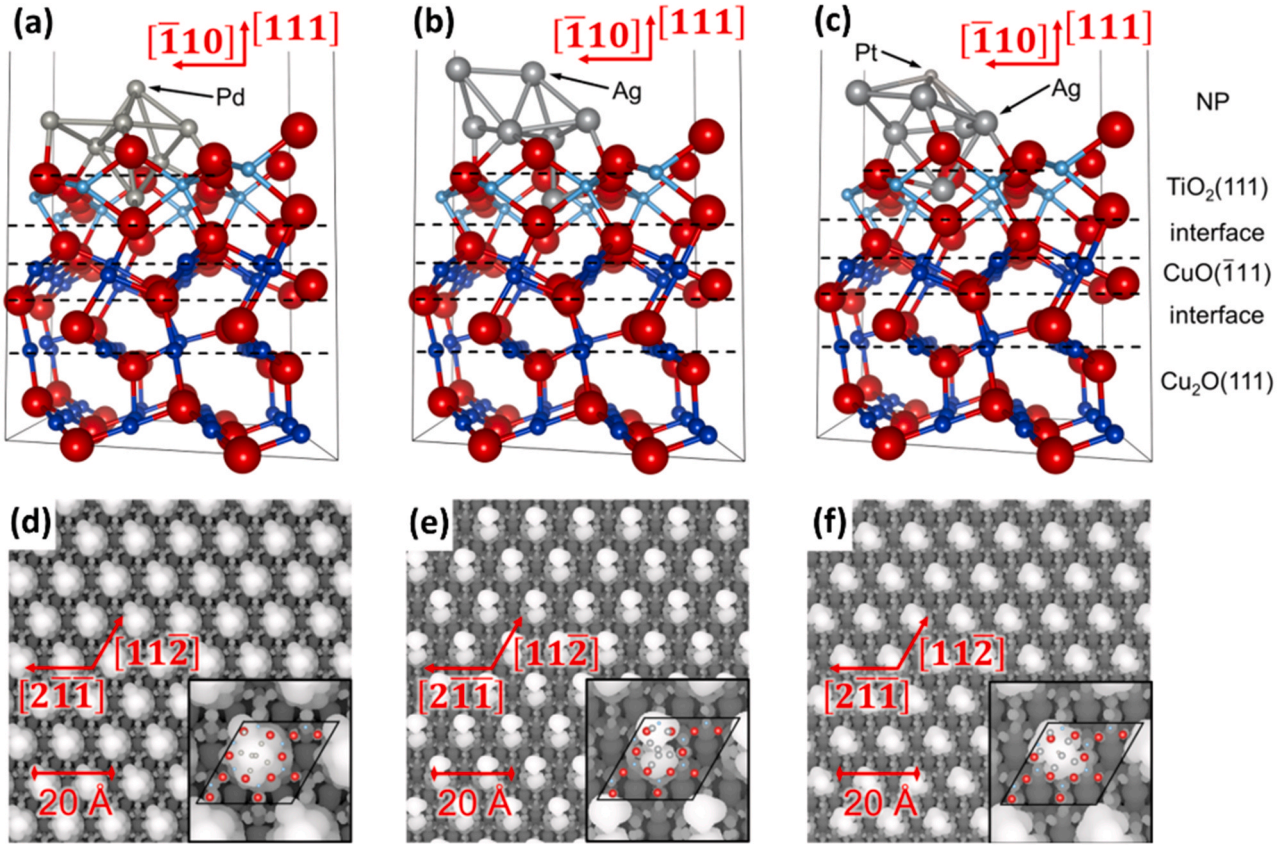

Fig. 8. (Top panels) Side view and (bottom panels) simulated scanning tunnelling microscopy (STM) images of the ternary $TiO_2(111)/CuO\left(\bar{1}11\right)/Cu_2O(111)$heteroepitaxial junction functionalised using (a and d) Pd_7; (b and e) Ag_7; and (c and f) Ag_6Pt nanoparticles. The ternary heterojunctions functionalised using the Pd_7, Ag_7 or Ag_6Pt nanoparticle are displayed using the ball-and-stick representation. The STM images were generated using a bias of: (d) $V = -0.5$ eV, (e) $V = -1.0$ eV and (f) $V = -1.5$ eV, an electron density of (d) $\rho = 0.0009$ e Å^{-3}, (e) $\rho = 0.0029$ e Å^{-3} and (f) $\rho = 0.0070$ e Å^{-3} as well as a tip distance of (d) $d = 2.25$ Å, (e) $d = 1.06$ Å and (f) $d = 2.17$ Å. Inset illustrate enlargement of the STM image for the surface unit cell. Crystallographic directions are indicated with respect to the $Cu_2O(111)$ substrate. O atoms are in red, Cu atoms are in dark blue, Ti atoms are in light blue and Pd, Ag or Pt atoms are in grey.

the adsorption energies (E_{ads}) for $Ag_7/TiO_2(111)/CuO\left(\bar{1}11\right)/Cu_2O$ (111) and $Ag_6Pt/TiO_2(111)/CuO\left(\bar{1}11\right)/Cu_2O(111)$, which display a strong shift in preference towards n-C_4H_9OH, with calculated $E_{ads} = -1.129$ eV and -1.053 eV, respectively, on the equatorial site of the NPs. However, the adsorption of the largest molecular weight alcohol on the least coordinated axial site of the NPs leads to a reduced binding energy by around 50% compared to its equatorial Ag counterpart position. Our calculations reveal that the decreasing order of strength of molecular adsorption is $E_{ads}(n\text{-}C_4H_9OH) > E_{ads}(C_2H_5OH) > E_{ads}(H_2)$ after replacing the axial Ag atom by Pt in Ag_7, as shown in Table S2.

Fig. 9a-c displays the thermodynamically most stable adsorption geometries for the interaction of the three molecules investigated computationally on the exposed facet of the heterostructure containing the noble metal clusters. We found that the diatomic H_2 molecule dissociates upon adsorption onto the equatorial Pd atoms of the nanoparticle, leading to the strongest interaction found in this work, see Fig. 9a. For this binding mode, our calculations suggest that the H atoms place themselves approximately along the [$\bar{2}$11] direction at either sides of the axial Pd atom. Thus, each H adatom forms a binuclear complex by coordinating both one equatorial and the axial Pd atom at the average distances of 1.71 Å and 1.78 Å. Fig. S15a-c shows the binding configurations of H_2, C_2H_5OH and n-C_4H_9OH on the most favourable adsorption sites of the $Pd_7/TiO_2(111)/CuO\left(\bar{1}11\right)/Cu_2O$ (111) sensor. For the heterostructure containing the Pd_7 clusters, H_2 interacts molecularly and nearly vertically at 1.75 Å above the 5-fold axial Pd site (see Fig. S15a), where it shows the least favourable adsorption observed on this material. C_2H_5OH moved outwards during the geometry optimisation from the initial equatorial site, forming a laterally coordinate bond of 2.27 Å to the axial Pd atom in its most stable adsorption configuration, as shown in Fig. S15b. The O atom from the largest molecular weight alcohol stays above the initial adsorption site, i.e. at 2.23 and 2.13 Å from the axial and equatorial Pd sites, see Fig. S14c. The Bader partition scheme reveals that H_2 lost electronic density upon adsorption, as shown in Table S2.

Fig. S15d-f illustrates the binding configurations of H_2, C_2H_5OH and n-C_4H_9OH on the most favourable adsorption sites of the $Ag_7/TiO_2(111)/CuO\left(\bar{1}11\right)/Cu_2O(111)$ sensor. The H_2 molecule adorbs molecularly at approximately 2.0 Å above the axial and to the side of the equatorial sites of the Ag_7 nanocluster, see Fig. S15d. The sensor can only exert a minor effect on the intramolecular H−H distance, with respect to the isolated H_2 molecule, which was calculated at 0.79 Å in both types of adsorption positions. We found that the C_2H_5OH molecule forms a vertical coordinate bond on the axial site with an O−Ag distance of 2.35 Å, which becomes 0.03 Å shorter on the equatorial adsorption position, as shown in Fig. S15e. Interestingly, n-C_4H_9OH moves laterally towards a surface O to form a hydrogen bond of 1.65 Å, resulting in the shortest O−Ag distance of 2.25 Å, which explains the largest binding energy calculated for this system in the equatorial site, see Fig. 9b. However, the largest molecular weight alcohol, n-butanol, interacts perpendicularly with the axial Ag atom at the slightly elongated distance of 2.31 Å. We observed that C_2H_5OH (n-C_4H_9OH) forms a vertical adsorption configuration on the heterostructure decorated using the Ag_7 nanoparticles.

For the molecular adsorptions on the sensor decorated by the Ag_7 nanoparticles, the Bader charge transfers were calculated between -0.039 and -0.074 e^-, see Table S2. These values indicate that the adsorbate loses electronic density to the heterojunction functionalised with the nanocluster, showing no clear correlation with the binding energies of the VOC and H_2 molecules. The small values of electron density flow that we have calculated for this material support the low sensitivity that it displayed in the experiments.

Fig. S15g-i depicts the structures of the molecular interactions with the surface sites of the heteroepitaxial material decorated with Ag_6Pt that released the largest adsorption energies. We found that H_2 remained perpendicularly atop the axial Pt atom at 1.91 Å, while it coordinated laterally the equatorial Ag site at the more elongated distance of 2.07 Å, which moved outwards upon adsorption, see Fig. S15g. Our DFT modelling suggests that C_2H_5OH prefers to stay parallel to the surface, binding both adsorption sites at the same distance of 2.29 Å, regardless of the different chemical nature of the metal atom, as shown in Fig. S15h. When n-C_4H_9OH

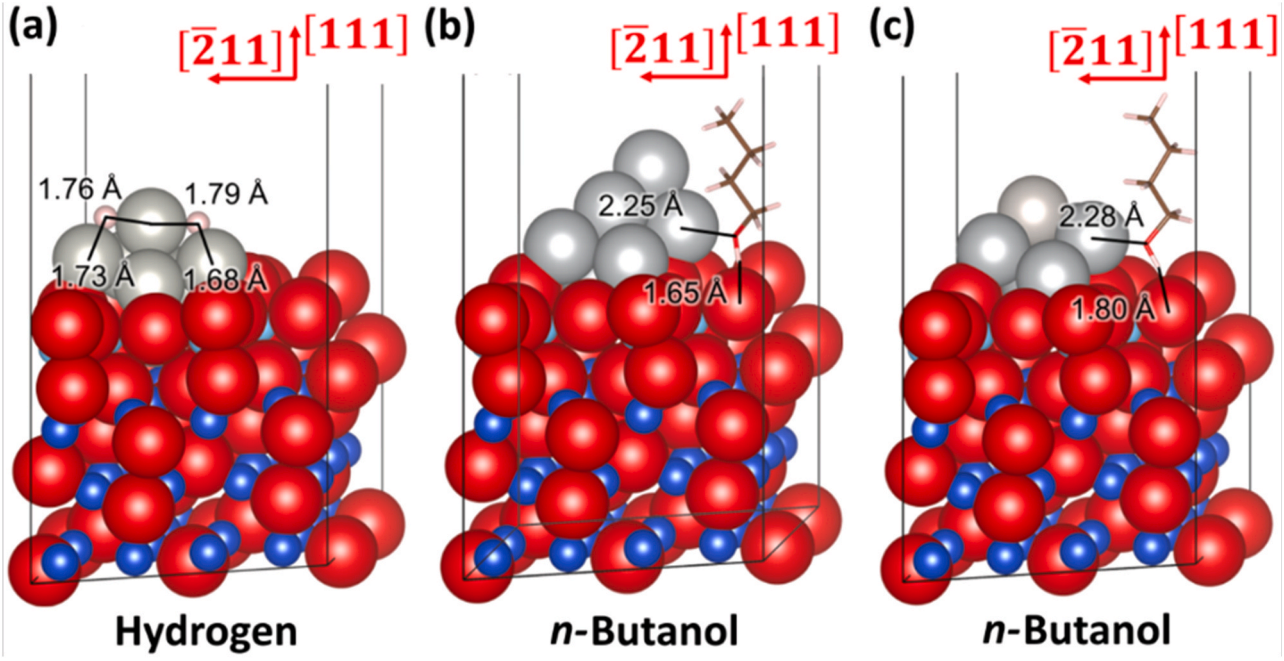

Fig. 9. Adsorption of: (a) H_2, and (b and c) n-C_4H_9OH on the $TiO_2(111)/CuO\left(\bar{1}11\right)/Cu_2O(111)$ heterostructure decorated with the Pd_7, Ag_7 and Ag_6Pt clusters, respectively. Interatomic distances are shown and crystallographic directions are indicated with respect to the $Cu_2O(111)$ substrate. The ternary heterojunctions functionalised using the Pd_7, Ag_7 or Ag_6Pt nanoparticles are displayed using the space-filling representation, whereas the adsorbates are shown using the stick representation. O atoms are in red, H atoms are in white, C atoms are in brown, Cu atoms are in dark blue, Ti atoms are in light blue and Pd, Ag and Pt atoms are in grey.

interacts with the axial or equatorial adsorption sites, the large alkyl radical positions itself perpendicularly to the surface. Fig. 9c illustrates that *n*-C_4H_9OH has a bidentate coordination mode with $Ag_6Pt/TiO_2(111)/CuO\left(\bar{1}11\right)/Cu_2O(111)$, by binding laterally to the equatorial Ag atom and by forming a hydrogen bond between the hydroxyl H and one of the surface O species. Moving this alcohol to the axial site forces a reduction of the interfacial O−Pt distance to 2.23 Å, which is nevertheless insufficient to counteract the loss of the hydrogen bond formed on the equatorial Ag site.

Our calculated charge transfers indicate that most of the adsorbates donate electron density to the sensor containing the Ag_6Pt nanoclusters, see Table S2. The electronic charges transferred by C_2H_5OH to the axial and equatorial sites of the nanoparticle are −0.085 and −0.098 e^-, respectively, displaying a direct correlation with the adsorption energies released in these positions. In contrast, *n*-C_4H_9OH donated −0.065 e^- in the most stable adsorption configuration on Ag_6Pt, a value that nearly doubled in the axial Pt position, leading to the largest charge transfer on this sensor. Despite H_2 having very close binding energies on both adsorption sites of Ag_6Pt, our models suggest that those interactions cause opposite flows of electron density, with the molecule receiving a charge of 0.011 e^- in the axial position. The density of states (DOS) are provided in Fig. S16 to validate the stability of the system.

A discussion of the adsorption geometries and charge transfers for the least favourable interactions can be found in the Text S4 (Supporting Information).

4. Conclusion

Changing the composition of the nanolayered CuO/Cu_2O structure with a total thickness of 60 nm by first depositing 20 nm of TiO_2 on top and subsequently Ag nanoparticles (5–15 nm of diameter), reduces the energy consumption of the final gas sensing device to below 1 nW. This fabrication process also allows tuning of the response spectrum of the sensor, thereby promoting the selectivity to 100 ppm of *n*-butanol vapours (response of over 200% at the operating temperature of 300 °C). In the case of AgPt functionalization, the response of the sensor increases even further to 220% for 100 ppm of *n*-butanol vapours at an operating temperature of 350 °C. In the case of Pd functionalization the selectivity of the sensor was changed from ethanol to hydrogen H_2, and the sensing performance was enhanced compared to the other compounds (response in the range between 400% and 600% at the lower operating temperature of 150–250 °C).

A tentative surface reaction mechanism explaining the sensing behaviour is proposed. At the interface of the $TiO_2/CuO/Cu_2O$ heterostructure, the ethanol molecule first suffers a reduction and is then combined with the holes present in CuO, producing the CH_3CHO intermediate, which finally reacts with the oxygen adsorbed on the *n-type* TiO_2 overlayer. We have used thermodynamic arguments derived from DFT calculations to rationalise the stability of the heteroepitaxial material before and after surface functionalization by noble metal nanoparticles. The adsorption energies agree and support the gas sensing experiments. This manuscript presents the methodology for nano-structuring and functionalizing of semiconducting oxides with tunable performances, as an alternative to clean room technology and micro-fabrication.

Declaration of Competing Interest

The authors declare that they have no known competing financial interests or personal relationships that could have appeared to influence the work reported in this paper.

Acknowledgements

The authors thank the WTSH and the EUSH for partially funding this project BAEW with (LPW-E/1.1.2/1486), Germany. This research was sponsored in part by the NATO Science for Peace and Security Programme (SPS) under grant G5634 “Advanced Electro-Optical Chemical Sensors” AMOXES. Dr. Lupan gratefully acknowledges PSL University, Chimie-ParisTech for invited professor positions in 2018 and 2019, CNRS Council for support as expert scientist at IRCP Chimie ParisTech, Paris, France. This research was sponsored partially by the German Research Foundation (DFG-Deutsche Forschungsgemeinschaft, Germany) under the schemes SFB1261, SFB1461 & AD 183/16–1. This work was financially supported by the German Research Foundation (DFG, Germany) via the research unit FOR 2093 "Memristive devices for neuronal systems" through project A2. The authors would like to thank Dr. Oleksandr Polonskyi for the technical assistance and for fruitful discussion. This work has used the ARCHER UK National Supercomputing Service (http://www.archer.ac.uk) provided via our membership of the UK’s HEC Materials Chemistry Consortium, funded by the Engineering and Physical Sciences Research Council (EPSRC grant EP/R029431). Work was also undertaken on ARC4, part of the High-Performance Computing facilities at the University of Leeds, United Kingdom. All data created during this research is provided in full in the results section of this paper.

Appendix A. Supporting information

Supplementary data associated with this article can be found in the online version at doi:10.1016/j.nanoen.2021.106241.

References

[1] F. Rasch, V. Postica, F. Schütt, Y.K. Mishra, A.S. Nia, M.R. Lohe, X. Feng, R. Adelung, O. Lupan, Highly selective and ultra-low power consumption metal oxide based hydrogen gas sensor employing graphene oxide as molecular sieve, Sens. Actuators B: Chem. 320 (2020), 128363, https://doi.org/10.1016/j.snb.2020.128363.

[2] F. Xue, L. Yang, M. Chen, J. Chen, X. Yang, L. Wang, L. Chen, C. Pan, Z.L. Wang, Enhanced photoresponsivity of the MoS_2-GaN heterojunction diode via the piezo-phototronic effect, NPG Asia Mater. 9 (2017) e418, https://doi.org/10.1038/am.2017.142.

[3] D. Zappa, V. Galstyan, N. Kaur, H.M.M. Munasinghe Arachchige, O. Sisman, E. Comini, “Metal oxide-based heterostructures for gas sensors”- A review, Anal. Chim. Acta 1039 (2018) 1–23, https://doi.org/10.1016/j.aca.2018.09.020.

[4] M. Hoppe, N. Ababii, V. Postica, O. Lupan, O. Polonskyi, F. Schütt, S. Kaps, L. F. Sukhodub, V. Sontea, T. Strunskus, F. Faupel, R. Adelung, (CuO-Cu_2O)/ZnO:Al heterojunctions for volatile organic compound detection, Sens. Actuators B Chem. 255 (2018) 1362–1375, https://doi.org/10.1016/j.snb.2017.08.135.

[5] S.M. Majhi, A. Mirzaei, H.W. Kim, S.S. Kim, T.W. Kim, Recent advances in energy-saving chemiresistive gas sensors: a review, Nano Energy 79 (2021), 105369, https://doi.org/10.1016/j.nanoen.2020.105369.

[6] J.-H. Kim, P. Wu, H.W. Kim, S.S. Kim, Highly selective sensing of CO, C_6H_6, and C_7H_8 gases by catalytic functionalization with metal nanoparticles, ACS Appl. Mater. Interfaces 8 (2016) 7173–7183, https://doi.org/10.1021/acsami.6b01116.

[7] N. Ababii, M. Hoppe, S. Shree, A. Vahl, M. Ulfa, T. Pauporté, B. Viana, V. Cretu, N. Magariu, V. Postica, V. Sontea, M.-I. Terasa, O. Polonskyi, F. Faupel, R. Adelung, O. Lupan, Effect of noble metal functionalization and film thickness on sensing properties of sprayed TiO_2 ultra-thin films, Sens. Actuators A Phys. 293 (2019) 242–258, https://doi.org/10.1016/j.sna.2019.04.017.

[8] A. Vahl, J. Dittmann, J. Jetter, S. Veziroglu, S. Shree, N. Ababii, O. Lupan, O. C. Aktas, T. Strunskus, E. Quandt, R. Adelung, S.K. Sharma, F. Faupel, The impact of O_2/Ar ratio on morphology and functional properties in reactive sputtering of metal oxide thin films, Nanotechnology 30 (2019), 235603, https://doi.org/10.1088/1361-6528/ab0837.

[9] V. Postica, A. Vahl, D. Santos-Carballal, T. Dankwort, L. Kienle, M. Hoppe, A. Cadi-Essadek, N.H. de Leeuw, M.-I. Terasa, R. Adelung, F. Faupel, O. Lupan, Tuning ZnO sensors reactivity toward volatile organic compounds via Ag doping and nanoparticle functionalization, ACS Appl. Mater. Interfaces 11 (2019) 31452–31466, https://doi.org/10.1021/acsami.9b07275.

[10] G. Niu, C. Zhao, H. Gong, Z. Yang, X. Leng, F. Wang, NiO nanoparticle-decorated SnO_2 nanosheets for ethanol sensing with enhanced moisture resistance, Microsyst. Nanoeng. 5 (2019) 21, https://doi.org/10.1038/s41378-019-0060-7.

[11] A. Vahl, O. Lupan, D. Santos-Carballal, V. Postica, S. Hansen, H. Cavers, N. Wolff, M.-I. Terasa, M. Hoppe, A. Cadi-Essadek, T. Dankwort, L. Kienle, N.H. de Leeuw, R. Adelung, F. Faupel, Surface functionalization of ZnO:Ag columnar thin films with AgAu and AgPt bimetallic alloy nanoparticles as an efficient pathway for highly sensitive gas discrimination and early hazard detection in batteries, J. Mater. Chem. A. 8 (2020) 16246–16264, https://doi.org/10.1039/D0TA03224G.

[12] H. Liu, W. Shen, X. Chen, A room temperature operated ammonia gas sensor based on Ag-decorated TiO_2 quantum dot clusters, RSC Adv. 9 (2019) 24519–24526, https://doi.org/10.1039/C9RA05439A.

[13] D. Zhao, M. Dai, Y. Zhao, H. Liu, Y. Liu, X. Wu, Improving electrocatalytic activities of $FeCo_2O_4$@$FeCo_2S_4$@PPy electrodes by surface/interface regulation, Nano Energy 72 (2020), 104715, https://doi.org/10.1016/j.nanoen.2020.104715.

[14] D. Zhao, H. Liu, X. Wu, Bi-interface induced multi-active MCo_2O_4@MCo_2S_4@PPy (M=Ni, Zn) sandwich structure for energy storage and electrocatalysis, Nano Energy 57 (2019) 363–370, https://doi.org/10.1016/j.nanoen.2018.12.066.

[15] D. Zhao, M. Dai, H. Liu, K. Chen, X. Zhu, D. Xue, X. Wu, J. Liu, Sulfur-induced interface engineering of hybrid $NiCo_2O_4$@$NiMo_2S_4$ structure for overall water splitting and flexible hybrid energy storage, Adv. Mater. Interfaces 6 (2019), 1901308, https://doi.org/10.1002/admi.201901308.

[16] H. Liu, D. Zhao, Y. Liu, P. Hu, X. Wu, H. Xia, Boosting energy storage and electrocatalytic performances by synergizing $CoMoO_4$@$MoZn_{22}$ core-shell structures, Chem. Eng. J. 373 (2019) 485–492, https://doi.org/10.1016/j.cej.2019.05.066.

[17] H. Wang, Y. Qu, H. Chen, Z. Lin, K. Dai, Highly selective n-butanol gas sensor based on mesoporous SnO_2 prepared with hydrothermal treatment, Sens. Actuators B Chem. 201 (2014) 153–159, https://doi.org/10.1016/j.snb.2014.04.049.

[18] New Jersey Department of Health, Right to Know Hazardous Substance Fact Sheet - n-butyl Alcohol, (2008). ⟨https://www.nj.gov/health/eoh/rtkweb/documents/fs/1330.pdf⟩. (Accessed January 15, 2020).

[19] I.S. Maddox, Production of n-butanol from whey filtrate using clostridium acetobutylicum N.C.I.B. 2951, Biotechnol. Lett. 2 (1980) 493–498, https://doi.org/10.1007/BF00129545.

[20] C.-L. Cheng, P.-Y. Che, B.-Y. Chen, W.-J. Lee, L.-J. Chien, J.-S. Chang, High yield bio-butanol production by solvent-producing bacterial microflora, Bioresour. Technol. 113 (2012) 58–64, https://doi.org/10.1016/j.biortech.2011.12.133.

[21] J. Huang, Y. Wu, C. Gu, M. Zhai, K. Yu, M. Yang, J. Liu, Large-scale synthesis of flowerlike ZnO nanostructure by a simple chemical solution route and its gas-sensing property, Sens. Actuators B Chem. 146 (2010) 206–212, https://doi.org/10.1016/j.snb.2010.02.052.

[22] O. Lupan, V. Cretu, V. Postica, N. Ababii, O. Polonskyi, V. Kaidas, F. Schütt, Y. K. Mishra, E. Monaico, I. Tiginyanu, V. Sontea, T. Strunskus, F. Faupel, R. Adelung, Enhanced ethanol vapour sensing performances of copper oxide nanocrystals with mixed phases, Sens. Actuators B Chem. 224 (2016) 434–448, https://doi.org/10.1016/j.snb.2015.10.042.

[23] V. Cretu, V. Postica, A.K. Mishra, M. Hoppe, I. Tiginyanu, Y.K. Mishra, L. Chow, N. H. de Leeuw, R. Adelung, O. Lupan, Synthesis, characterization and DFT studies of zinc-doped copper oxide nanocrystals for gas sensing applications, J. Mater. Chem. A 4 (2016) 6527–6539, https://doi.org/10.1039/C6TA01355D.

[24] L.-J. Zhou, Y.-C. Zou, J. Zhao, P.-P. Wang, L.-L. Feng, L.-W. Sun, D.-J. Wang, G.-D. Li, Facile synthesis of highly stable and porous Cu_2O/CuO cubes with enhanced gas sensing properties, Sens. Actuators B Chem. 188 (2013) 533–539, https://doi.org/10.1016/j.snb.2013.07.059.

[25] H. Haberland, M. Karrais, M. Mall, Y. Thurner, Thin films from energetic cluster impact: a feasibility study, J. Vac. Sci. Technol. A Vac. Surf. Film 10 (1992) 3266–3271, https://doi.org/10.1116/1.577853.

[26] A. Vahl, J. Strobel, W. Reichstein, O. Polonskyi, T. Strunskus, L. Kienle, F. Faupel, Single target sputter deposition of alloy nanoparticles with adjustable composition via a gas aggregation cluster source, Nanotechnology 28 (2017), 175703, https://doi.org/10.1088/1361-6528/aa66ef.

[27] S. Veziroglu, J. Hwang, J. Drewes, I. Barg, J. Shondo, T. Strunskus, O. Polonskyi, F. Faupel, O.C. Aktas, PdO nanoparticles decorated TiO_2 film with enhanced photocatalytic and self-cleaning properties, Mater. Today Chem. 16 (2020), 100251, https://doi.org/10.1016/j.mtchem.2020.100251.

[28] O. Lupan, V. Postica, M. Hoppe, N. Wolff, O. Polonskyi, T. Pauporté, B. Viana, O. Majérus, L. Kienle, F. Faupel, R. Adelung, PdO/PdO_2 functionalized ZnO:Pd films for lower operating temperature H_2 gas sensing, Nanoscale 10 (2018) 14107–14127, https://doi.org/10.1039/C8NR03260B.

[29] O. Lupan, V. Cretu, V. Postica, O. Polonskyi, N. Ababii, F. Schütt, V. Kaidas, F. Faupel, R. Adelung, Non-planar nanoscale p–p heterojunctions formation in $Zn_xCu_{1-x}O_y$ nanocrystals by mixed phases for enhanced sensors, Sens. Actuators B Chem. 230 (2016) 832–843, https://doi.org/10.1016/j.snb.2016.02.089.

[30] G. Kresse, J. Hafner, Ab initio molecular dynamics for liquid metals, Phys. Rev. B 47 (1993) 558–561, https://doi.org/10.1103/PhysRevB.47.558.

[31] G. Kresse, J. Hafner, Ab initio molecular-dynamics simulation of the liquid-metal–amorphous-semiconductor transition in germanium, Phys. Rev. B. 49 (1994) 14251–14269, https://doi.org/10.1103/PhysRevB.49.14251.

[32] G. Kresse, J. Furthmüller, Efficient iterative schemes for ab initio total-energy calculations using a plane-wave basis set, Phys. Rev. B. 54 (1996) 11169–11186, https://doi.org/10.1103/PhysRevB.54.11169.

[33] G. Kresse, J. Furthmüller, Efficiency of ab-initio total energy calculations for metals and semiconductors using a plane-wave basis set, Comput. Mater. Sci. 6 (1996) 15–50, https://doi.org/10.1016/0927-0256(96)00008-0.

[34] J.P. Perdew, K. Burke, M. Ernzerhof, Generalized gradient approximation made simple [Phys. Rev. Lett. 77, 3865 (1996)], Phys. Rev. Lett. 78 (1997) 1396, https://doi.org/10.1103/PhysRevLett.78.1396.

[35] J.P. Perdew, K. Burke, M. Ernzerhof, Generalized gradient approximation made simple, Phys. Rev. Lett. 77 (1996) 3865–3868, https://doi.org/10.1103/PhysRevLett.77.3865.

[36] S. Grimme, J. Antony, S. Ehrlich, H. Krieg, A consistent and accurate ab initio parametrization of density functional dispersion correction (DFT-D) for the 94 elements H-Pu, J. Chem. Phys. 132 (2010), 154104, https://doi.org/10.1063/1.3382344.

[37] S. Grimme, S. Ehrlich, L. Goerigk, Effect of the damping function in dispersion corrected density functional theory, J. Comput. Chem. 32 (2011) 1456–1465, https://doi.org/10.1002/jcc.21759.

[38] B. Farkaš, D. Santos-Carballal, A. Cadi-Essadek, N.H. de Leeuw, A DFT+U study of the oxidation of cobalt nanoparticles: Implications for biomedical applications, Materialia 7 (2019), 100381, https://doi.org/10.1016/j.mtla.2019.100381.

[39] M.J. Ungerer, D. Santos-Carballal, A. Cadi-Essadek, C.G.C.E. van Sittert, N.H. de Leeuw, Interaction of H_2O with the platinum Pt (001), (011), and (111) surfaces: a density functional theory study with long-range dispersion corrections, J. Phys. Chem. C 123 (2019) 27465–27476, https://doi.org/10.1021/acs.jpcc.9b06136.

[40] L.M. Botha, D. Santos-Carballal, U. Terranova, M.G. Quesne, M.J. Ungerer, C.G.C. E. van Sittert, N.H. de Leeuw, Mixing thermodynamics and electronic structure of the $Pt_{1-x}Ni_x$ ($0 \leq x \leq 1$) bimetallic alloy, RSC Adv. 9 (2019) 16948–16954, https://doi.org/10.1039/C9RA02320H.

[41] D. Santos-Carballal, P.E. Ngoepe, N.H. de Leeuw, Ab initio investigation of the thermodynamics of cation distribution and of the electronic and magnetic structures in the LiMn2O4 spinel, Phys. Rev. B. 97 (2018), 085126, https://doi.org/10.1103/PhysRevB.97.085126.

[42] S. Posada-Pérez, D. Santos-Carballal, U. Terranova, A. Roldan, F. Illas, N.H. de Leeuw, CO_2 interaction with violarite ($FeNi_2S_4$) surfaces: a dispersion-corrected DFT study, Phys. Chem. Chem. Phys. 20 (2018) 20439–20446, https://doi.org/10.1039/C8CP03430C.

[43] V. Postica, A. Vahl, J. Strobel, D. Santos-Carballal, O. Lupan, A. Cadi-Essadek, N. H. De Leeuw, F. Schütt, O. Polonskyi, T. Strunskus, M. Baum, L. Kienle, R. Adelung, F. Faupel, Tuning doping and surface functionalization of columnar oxide films for volatile organic compounds sensing: experiments and theory, J. Mater. Chem. A. 6 (2018) 23669–23682, https://doi.org/10.1039/C8TA08985J.

[44] L. Reguera, N.L. López, J. Rodríguez-Hernández, M. González, C.E. Hernandez-Tamargo, D. Santos-Carballal, N.H. de Leeuw, E. Reguera, Synthesis, crystal structures, and properties of zeolite-Like $T_3(H_3O)_2M(CN)_6]_2{\cdot}uH_2O$ (T = Co, Zn; M = Ru, Os), Eur. J. Inorg. Chem. 2017 (2017) 2980–2989, https://doi.org/10.1002/ejic.201700278.

[45] B. Ramogayana, D. Santos-Carballal, P.A. Aparicio, M.G. Quesne, K.P. Maenetja, P. E. Ngoepe, N.H. de Leeuw, Ethylene carbonate adsorption on the major surfaces of lithium manganese oxide $Li_{1-x}Mn_2O_4$ spinel ($0.000 < x < 0.375$): a DFT+ U -D3 study, Phys. Chem. Chem. Phys. 22 (2020) 6763–6771, https://doi.org/10.1039/C9CP05658K.

[46] P.E. Blöchl, Projector augmented-wave method, Phys. Rev. B 50 (1994) 17953–17979, https://doi.org/10.1103/PhysRevB.50.17953.

[47] G. Kresse, D. Joubert, From ultrasoft pseudopotentials to the projector augmented-wave method, Phys. Rev. B 59 (1999) 1758–1775, https://doi.org/10.1103/PhysRevB.59.1758.

[48] D. Sheppard, R. Terrell, G. Henkelman, Optimization methods for finding minimum energy paths, J. Chem. Phys. 128 (2008), 134106, https://doi.org/10.1063/1.2841941.

[49] M.R. Hestenes, E. Stiefel, Methods of conjugate gradients for solving linear systems, J. Res. Natl. Bur. Stan. 49 (1952) 409, https://doi.org/10.6028/jres.049.044.

[50] V.I. Anisimov, M.A. Korotin, J. Zaanen, O.K. Andersen, Spin bags, polarons, and impurity potentials in $La_{2-x}Sr_xCuO_4$ from first principles, Phys. Rev. Lett. 68 (1992) 345–348, https://doi.org/10.1103/PhysRevLett.68.345.

[51] S.L. Dudarev, G.A. Botton, S.Y. Savrasov, C.J. Humphreys, A.P. Sutton, Electron-energy-loss spectra and the structural stability of nickel oxide: an LSDA+U study, Phys. Rev. B. 57 (1998) 1505–1509, https://doi.org/10.1103/PhysRevB.57.1505.

[52] I. de, P.R. Moreira, F. Illas, R.L. Martin, Effect of Fock exchange on the electronic structure and magnetic coupling in NiO, Phys. Rev. B. 65 (2002), 155102, https://doi.org/10.1103/PhysRevB.65.155102.

[53] C.E. Calderon, J.J. Plata, C. Toher, C. Oses, O. Levy, M. Fornari, A. Natan, M. J. Mehl, G. Hart, M. Buongiorno Nardelli, S. Curtarolo, The AFLOW standard for high-throughput materials science calculations, Comput. Mater. Sci. 108 (2015) 233–238, https://doi.org/10.1016/j.commatsci.2015.07.019.

[54] W. Setyawan, S. Curtarolo, High-throughput electronic band structure calculations: challenges and tools, Comput. Mater. Sci. 49 (2010) 299–312, https://doi.org/10.1016/j.commatsci.2010.05.010.

[55] W. Setyawan, R.M. Gaume, S. Lam, R.S. Feigelson, S. Curtarolo, High-throughput combinatorial database of electronic band structures for inorganic scintillator materials, ACS Comb. Sci. 13 (2011) 382–390, https://doi.org/10.1021/co200012w.

[56] S. Wang, Z. Wang, W. Setyawan, N. Mingo, S. Curtarolo, Assessing the thermoelectric properties of sintered compounds via high-throughput ab-initio calculations, Phys. Rev. X. 1 (2011) 1–8, https://doi.org/10.1103/PhysRevX.1.021012.

[57] R.H. Taylor, F. Rose, C. Toher, O. Levy, K. Yang, M. Buongiorno Nardelli, S. Curtarolo, A RESTful API for exchanging materials data in the AFLOWLIB.org consortium, Comput. Mater. Sci. 93 (2014) 178–192, https://doi.org/10.1016/j.commatsci.2014.05.014.

[58] O.K. Andersen, Electronic structure of the fcc transition metals Ir, Rh, Pt, and Pd, Phys. Rev. B 2 (1970) 883–906, https://doi.org/10.1103/PhysRevB.2.883.

[59] W. Speier, J.C. Fuggle, R. Zeller, B. Ackermann, K. Szot, F.U. Hillebrecht, M. Campagna, Bremsstrahlung isochromat spectra and density-of-states calculations for the 3d and 4d transition metals, Phys. Rev. B. 30 (1984) 6921–6930, https://doi.org/10.1103/PhysRevB.30.6921.

[60] H.J. Monkhorst, J.D. Pack, Special points for Brillouin-zone integrations, Phys. Rev. B 13 (1976) 5188–5192, https://doi.org/10.1103/PhysRevB.13.5188.

[61] M. Methfessel, A.T. Paxton, High-precision sampling for Brillouin-zone integration in metals, Phys. Rev. B 40 (1989) 3616–3621, https://doi.org/10.1103/PhysRevB.40.3616.

[62] N.D. Mermin, Thermal properties of the inhomogeneous electron gas, Phys. Rev. 137 (1965) A1441–A1443, https://doi.org/10.1103/PhysRev.137.A1441.

[63] P.E. Blöchl, O. Jepsen, O.K. Andersen, Improved tetrahedron method for Brillouin-zone integrations, Phys. Rev. B 49 (1994) 16223–16233, https://doi.org/10.1103/PhysRevB.49.16223.

[64] W. Li, X. Yan, A.G. Aberle, S. Venkataraj, Effect of sodium diffusion on the properties of CIGS solar absorbers prepared using elemental Se in a two-step process, Sci. Rep. 9 (2019) 2637, https://doi.org/10.1038/s41598-019-39283-2.
[65] J.-T. Fonné, E. Burov, E. Gouillart, S. Grachev, H. Montigaud, D. Vandembroucq, Interdiffusion between silica thin films and soda-lime glass substrate during annealing at high temperature, J. Am. Ceram. Soc. 102 (2019) 3341–3353, https://doi.org/10.1111/jace.16154.
[66] J.F. Moulder, W.F. Stickle, P.E. Sobol, K.D. Bomben, Handbook of X-ray photoelectron spectroscopy, Perkin-Elmer corporation, Eden Prairie, Minn. (1992). ⟨https://www.cnyn.unam.mx/~wencel/XPS/MANXPS.pdf⟩.
[67] C.J.P. Alexander V. Naumkin, Anna Kraut-Vass, Stephen W. Gaarenstroom, NIST X-ray Photoelectron Spectroscopy Database, NIST X-Ray Photoelectron Spectrosc. Database, NIST Stand. Ref. Database 20, Version 4.1. 2000. https://doi.org/10.18434/T4T88K.
[68] A. Sahai, N. Goswami, S.D. Kaushik, S. Tripathi, Cu/Cu_2O/CuO nanoparticles: novel synthesis by exploding wire technique and extensive characterization, Appl. Surf. Sci. 390 (2016) 974–983, https://doi.org/10.1016/j.apsusc.2016.09.005.
[69] K.A. Willets, R.P. Van Duyne, Localized surface plasmon resonance spectroscopy and sensing, Annu. Rev. Phys. Chem. 58 (2007) 267–297, https://doi.org/10.1146/annurev.physchem.58.032806.104607.
[70] J.R. Ferraro, K. Nakamoto, Basic Theory, in: J.R. Ferraro, K.B.T.-I.R.S. Nakamoto (Eds.), Introd. Raman Spectrosc., Elsevier, Boston, 1994, pp. 1–94, https://doi.org/10.1016/B978-0-12-253990-9.50005-7.
[71] C.K. Law, Resonance response of the quantum vacuum to an oscillating boundary, Phys. Rev. Lett. 73 (1994) 1931–1934, https://doi.org/10.1103/PhysRevLett.73.1931.
[72] F. Wooten, Optical Properties of Solids, Academic Press, New York, NY, 1972. ⟨http://cds.cern.ch/record/268948⟩.
[73] A.E. Rakhshani, Preparation, characteristics and photovoltaic properties of cuprous oxide—a review, Solid. State Electron. 29 (1986) 7–17, https://doi.org/10.1016/0038-1101(86)90191-7.
[74] B. Balamurugan, I. Aruna, B.R. Mehta, S.M. Shivaprasad, Size-dependent conductivity-type inversion in Cu_2O nanoparticles, Phys. Rev. B. 69 (2004), 165419, https://doi.org/10.1103/PhysRevB.69.165419.
[75] V. Postica, A. Vahl, N. Magariu, M.-I. Terasa, M. Hoppe, B. Viana, P. Aschehoug, T. Pauporté, I. Tiginyanu, O. Polonskyi, V. Sontea, L. Chow, L. Kienle, R. Adelung, F. Faupel, O. Lupan, Enhancement in UV sensing properties of ZnO:Ag nanostructured films by surface functionalization with noble metalic and bimetallic nanoparticles, J. Eng. Sci. XXV (2018) 41–51, https://doi.org/10.5281/zenodo.2557280.
[76] M. Mathew, P.V. Shinde, R. Samal, C.S. Rout, A review on mechanisms and recent developments in p-n heterojunctions of 2D materials for gas sensing applications, J. Mater. Sci. 56 (2021) 9575–9604, https://doi.org/10.1007/s10853-021-05884-4.
[77] H. Xuemei, S. Yukun, B. Bo, Fabrication of cubic p-n heterojunction-like NiO/In_2O_3 composite microparticles and their enhanced gas sensing characteristics, J. Nanomater. 2016 (2016) 1–9, https://doi.org/10.1155/2016/7589028.
[78] D.E.P. Vanpoucke, G. Brocks, Formation of Pt-induced Ge atomic nanowires on Pt/Ge(001): a density functional theory study, Phys. Rev. B. 77 (2008), 241308, https://doi.org/10.1103/PhysRevB.77.241308.
[79] J. Tersoff, D.R. Hamann, Theory of the scanning tunneling microscope, Phys. Rev. B 31 (1985) 805–813, https://doi.org/10.1103/PhysRevB.31.805.

Oleg Lupan received his Ph.D. from the Institute of Applied Physics, Academy of Sciences of Moldova (ASM) in 2005. He then held post-doctoral research positions at the CNRS, France and at the University of Central Florida, USA. Prof Lupan received his habilitation from the Institute of Electronic Engineering and Nanotechnologies, ASM in 2011 and then became a Professor in Solid State Electronics and Nanoelectronics at the Technical University of Moldova (TUM). Prof Lupan is a frequent visiting scholar in the research group "Functional Nanomaterials" of Prof Adelung, Germany. His current research interests include nanosensors, optoelectronic devices, nanotechnologies, and nanodevices. https://utm.md/

Nicolai Ababii is a current Ph.D. candidate in the research group "Nanotechnology and Nanosensors" of Prof. Dr. Lupan at the Department of Microelectronics and Biomedical Engineering, Technical University of Moldova (TUM). He gained experience controlling the surface properties of copper oxide nanocomposites during his Engineering degree. He received his M.Sc. in Microelectronics and Nanotechnologies from TUM in 2016. He was awarded a fellowship for the 2018–2019 academic year by the Moldovan Government in recognition of his excellent Ph.D. studies. His current research interests are nanostructuring of semiconducting oxide thin films and nanowires for gas sensors. https://utm.md/

David Santos-Carballal received his BSc in Chemistry from University of Havana, Cuba, in 2007 and completed his MRes and PhD at University College London, UK. He was a Post-doctoral Research Associate at Cardiff University and is currently a Senior Research Fellow at the School of Chemistry of the University of Leeds, where he uses density functional theory-based calculations to understand the solid state and surface chemistry of materials for catalysis and energy applications. Dr Santos-Carballal was awarded a prestigious Post-doctoral Fellowship by the DST and NRF of South Africa in 2016, to carry out research at University of Limpopo. https://eps.leeds.ac.uk/chemistry

Maik-Ivo Terasa is currently working as a Ph.D. student with Prof. Dr. Rainer Adelung at the Functional Nano-materials Chair at the Institute for Materials Science, Faculty of Engineering, University of Kiel, Germany. He received his M.Sc. degree in Materials Science and Engineering in 2017 from the Kiel University. His current research is focused on the junction of memristive and sensitive components for neuromorphic applications.

Nicolae Magariu is currently a Ph.D. candidate in the group "Nanotechnology and Nanosensors" of Prof. Dr. Lupan, at the Technical University of Moldova (TUM). He worked in the field of metal oxides and their surface modification during his Engineering and Master's degree diplomas at TUM. His current research interests are nanostructuring of semiconducting oxide thin films, gas sensors, and the development of UV photodetectors. He was awarded a fellowship for the 2019-2020 academic year by the Moldovan Government in recognition of his excellent Ph.D. studies. http://mib.utm.md/

Dario Zappa received his B.Sc. (2006) and M.Sc. (2009) in Electronic Engineering, and his Ph.D. (2013) in Material Science from University of Brescia. Presently, he is Assistant Professor at SENSOR Lab (Brescia, Italy). His research activities are focused on the synthesis and characterization of nanostructured metal oxides for different applications, including gas sensors, e-noses and thermoelectric devices. In the last few years, he was involved in many international (European and NATO funded) and national projects (MIUR, Regional). Since 2012 he is lecturer in Physics at the University of Brescia.

Elisabetta Comini received her first degree in Physics from the University of Pisa and her Ph.D. in Material Science from the University of Brescia. In 2016 she became Professor in Physics of Matter at Brescia University. She was chair of MRS fall meeting 2013. She has a high productivity confirmed by the numerous publications on international journals (>390) and the high number of invited presentations at conferences. EC is a researcher specialist in metal oxides, particularly nanowires, thin films and the measurement of their electronic, functional and structural properties. EC is the director of SENSOR laboratory (Brescia University, http://sensor.unibs.it)

Thierry Pauporté is director of research at the Centre National de la Recherche Scientifique (CNRS) in France and works at Chimie-Paristech-PSL University. He is graduated in Chemistry from the École Normale Supérieure de Lyon. He received his Ph.D. in physical chemistry from Montpellier II University, France, in 1995. He works on the synthesis, characterization and understanding of fundamental chemical and physical properties of oxide and halide perovskite films and nanostructures. The applications of these materials and structures include light emitting diodes, perovskite solar cells, dye-sensitized solar cells, nanosensors, photodetectors, photocatalysis, wettability and fouling. Website : www.pauporte group.com

Leonard Siebert is a Ph.D. student at the Functional Nanomaterials Chair, Institute for Materials Science, Kiel University, Germany. In his work, he focuses on novel fabrication techniques for extreme polymer composites, additive manufacturing and metal oxide semiconductor gas sensors. Having developed multiple 3D-printing setups, he seeks to apply innovative and unconventional means for manufacturing new materials.

Franz Faupel received his Ph.D. in physics from the University of Göttingen in 1985. He was postdoctoral fellow at the IBM Research Center Yorktown Heights and received his habilitation in 1992. Since 1994, he holds the Chair for Multicomponent Materials at Kiel University. He is Chairman of the North German Initiative Nanotechnology and has served on various editorial boards including Journal of Materials Research, SN Applied Sciences, Materials, Applied Physics Letters, and Journal of Applied Physics. He published more than 360 papers (h index 50, Web of Sciences). His research interests include functional nanocomposites, magnetoelectric sensors, photocatalysis, and plasma deposition.

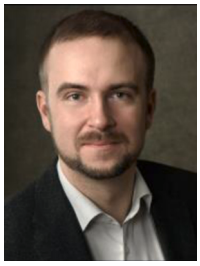

Alexander Vahl studied Materials Science at Kiel University (2009–2014) and completed his dissertation in 2019 at the Chair of Prof. F. Faupel (Multicomponent Materials) on the topic of memristive switching and memsensor devices. Since 2019 he continued his work as postdoc on the topic of functional nanocomposites for neuromorphic engineering and neurotronics, which he pursues as independent principal investigator at Kiel University and with a PostDoc stay in the group of Prof. P. Milani (Universita degli studi di Milano). His field of study includes memristive and memsensitive thin film devices with a special focus on nanoparticle composites.

Sandra Hansen is a Post-Doc and Habilitation Candidate at the Functional Nanomaterials Chair, at the Department of Engineering of Christian-Albrechts-University, Kiel, Germany. She received her Ph.D. in Materials Science in 2017 from Kiel University and was awarded a prize for the best dissertation of that year. She worked at SLAC, Stanford University, USA, in the field of full silicon anodes for Lithium-Ion Batteries. Since 2017, she is leading an independent research group on battery technology and development at the Functional Nanomaterials Chair. Her research focuses on materials for current and post Li-ion batteries, memristive devices and battery electrolytes.

Nora H. de Leeuw is a prominent scientist in the field of computational chemistry of complex materials. Research interests include the computer-aided design of energy materials, e.g. sustainable catalysts for the conversion of carbon dioxide to fuels and chemicals under mild reaction conditions, and biocompatible materials for tissue engineering applications. De Leeuw holds professorial appointments at the Universities of Leeds, UK, and Utrecht, the Netherlands, and she has been awarded research fellowships by the EPSRC, Royal Society and AWE. She is a Royal Society Merit Award holder, Fellow of the Learned Society of Wales, and Member of Academia Europaea.

Rainer Adelung is full professor and chairholder of the Functional Nanomaterials group established in 2007 at the Institute for Materials Science, Kiel University, Germany. He received his Ph.D. (rer. nat.) in physics in 2000 from the Institute of Experimental and Applied Physics, Kiel University, and during 2001–2002 he was at Case Western Reserve University in Cleveland (USA) as Feodor Lynen (Alexander von Humboldt) research fellow. In 2006 he finished his Habilitation at the Institute for Materials Science in Kiel and then continued as Heisenberg Professor (DFG grant) starting his own Functional Nanomaterials group in 2007. More information at https://www.tf.uni-kiel.de/matwis/fnano/de.